Gondwana Research 131 (2024) 317–342

Contents lists available at ScienceDirect

Gondwana Research

journal homepage: www.elsevier.com/locate/gr

Zircon U-Pb and Lu-Hf isotopes reveal the crustal evolution of the SW Angolan Shield (Congo Craton)

Ezequiel Ferreira [a,b,c,*], Jérémie Lehmann [d], José Feliciano Rodrigues [e], Ben Hayes [f], Enrique Merino-Martínez [b], Lorenzo Milani [g], Grant M. Bybee [f], Trishya M. Owen Smith [d], José Luis García-Lobón [b], Colombo C. G. Tassinari [h], Henriette Ueckermann [d], Kei Sato [h], Paulo Bravo Silva [a], João Correia [a], José Labaredas [a], Laurent Duarte [a,i], Mmasetena Anna Molekwa [d], José Manuel [j,k], Américo da Mata Lourenço Victorino [j]

[a] UTE PLANAGEO-LNEG, Estrada da Portela, Bairro do Zambujal, 2610-999 Amadora, Portugal
[b] IGME-CSIC (Instituto Geológico y Minero de España-Consejo Superior de Investigaciones Científicas), 28760 Tres Cantos, Madrid, Spain
[c] Instituto Dom Luiz, Faculty of Sciences, University of Lisbon, 1749-016 Lisbon, Portugal
[d] Department of Geology, University of Johannesburg, Auckland Park, Johannesburg, 2006, South Africa
[e] Laboratório Nacional de Energia e Geologia, Rua da Amieira, 4466-901 São Mamede de Infesta, Portugal
[f] School of Geosciences, University of the Witwatersrand, Johannesburg, 2050, South Africa
[g] Department of Geology, University of Pretoria, Private Bag X20, Hatfield 0028, South Africa
[h] Centro de Pesquisas Geocronológicas (CPGeo), Instituto de Geociências, Universidade de São Paulo, São Paulo 05422-970, Brazil
[i] Omatapalo - Engenharia & Construção, S.A., Bairro do Tchioco, Zona Industrial II, Lubango, Angola
[j] Instituto Geológico de Angola, Rua 311, Centralidade do Kilamba, Luanda, Angola
[k] Faculdade de Ciências Naturais, Universidade A. Neto, Av. 4 de Fevereiro, 71A, Luanda, Angola

ARTICLE INFO

Article history:
Received 23 February 2024
Revised 27 February 2024
Accepted 24 March 2024
Available online 28 March 2024
Handling Editor: A. Festa

Keywords:
SW Angolan Shield
Archean to Mesoproterozoic
Detrital and igneous zircon
U-Pb and Lu-Hf isotopes
Crustal evolution

ABSTRACT

The crustal evolution of the Angolan Shield (AS) remains poorly constrained. To address this, we analysed U-Pb and Lu-Hf isotopes in detrital and igneous zircons to investigate the age and provenance of extensive sedimentary strata in southwestern Angola and use it as a proxy to gain insight into the Archean to Mesoproterozoic evolution of the region.

Mesoproterozoic maximum depositional ages for the Iona (<1323 ± 13 Ma), Ompupa (<1215 ± 13 Ma), and Cahama (<1184 ± 23 Ma) siliciclastics challenge previous correlations with the Paleoproterozoic Chela Group. Provenance analysis reveals that the Mesoproterozoic strata were derived internally from the AS.

Our combined dataset indicates that the widespread Eburnean magmatism (~2.05–1.93 Ga) resulted from reworking of Archean crust, possibly in collision orogens. A major increase in the $\varepsilon Hf_{(i)}$ and $\varepsilon Nd_{(i)}$ values at ~ 1.87–1.73 Ga indicates a change in geodynamics, with magmatism of the Epupa–Namibe Metamorphic Complex (ENMC) generated in an extensional accretionary orogen at the southern margin of the Eburnean–Archean crustal block. Magmatism resumed in the Mesoproterozoic (~1.56–1.50 Ga), with suprachondritic $\varepsilon Hf_{(i)}$ values indicating significant juvenile addition. The Kunene Complex (KC: ~1.50–1.36 Ga) anorthosite-mangerite-charnockite-granite magmatism displays variable $\varepsilon Hf_{(i)}$ and $\varepsilon Nd_{(i)}$ values, consistent with mixing between reworked ENMC-crust and juvenile melts in a long-lived accretionary orogen back-arc region. Post-KC (~1.36–1.30 Ga) magmatism shows an increased juvenile contribution, potentially linked to partial melting of ENMC and ~ 1.56–1.50 Ga juvenile crust during an orogenic event, or alternatively, related to renewed slab retreat and back-arc extension. The Hf isotopic compositions of ~ 1.29–1.18 Ga zircons are compatible with a renewed input from the depleted mantle and/or reworking of the earlier ~ 1.56–1.50 Ga juvenile crust. Emplacement of ~ 1.13–1.10 Ga mafic dikes/sills marks the end of Mesoproterozoic magmatism in the AS. Our new data enhance our understanding of the Archean to Mesoproterozoic crustal evolution of the AS.

* Corresponding author currently at: IGME-CSIC (Instituto Geológico y Minero de España-Consejo Superior de Investigaciones Científicas), 28760 Tres Cantos, Madrid, Spain.
E-mail addresses: ezequiel.geo@gmail.com, ej.ferreira@igme.es (E. Ferreira).

https://doi.org/10.1016/j.gr.2024.03.010
1342-937X/

1. Introduction

The Angolan Shield (AS), the southwestern portion of the Congo Craton, remains one of the least studied cratonic blocks in southern Africa. Although the Mesoproterozoic Kunene AMCG (anorthosite-mangerite-charnockite-granite) Complex (KC, 1500–1370 Ma) and its Paleoproterozoic basement have been relatively well studied over the past two decades (Baxe, 2007; Bybee et al., 2019; Campeny et al., 2023; Ernst et al., 2013; Hayes et al., 2022; Jelsma et al., 2018; Langa, 2019; Lehmann et al., 2020, 2023; Mayer et al., 2004; McCourt et al., 2013; Milani et al., 2022; Pereira et al., 2011; Salminen et al., 2018), the extensive Proterozoic supracrustal sequences in this region continue to be poorly documented, hindering a more comprehensive understanding of the geological evolution of the AS.

One of the most remarkable features of the southwestern AS is the presence of extensive (up to 1000 km^2) outliers of commonly undeformed sedimentary rocks, previously known as the Chela Group (Correia, 1976; Figs. 1 and 2). These were thought to be correlated with the Neoproterozoic–Cambrian Damara Supergroup in Namibia (Beetz, 1933; Carvalho, 1972; Correia, 1976; Kröner and Correia, 1980; Mouta, 1954; Torquato, 1971; Vale, 1973a, 1973b), or to be Mesoproterozoic (Carvalho et al., 1987; Torquato, 1974; Torquato and Salgueiro, 1977), or even Paleoproterozoic (Carvalho and Alves, 1993; Pereira et al., 2011). However, recent U-Pb dating, and an Angolan government-sponsored geological mapping program (PLANAGEO), have revealed that the sedimentary rocks from the Humpata Plateau are younger than 1800 Ma (McCourt et al., 2013) and older than ~ 1500 Ma mafic sills in the region (Ernst et al., 2013). The sedimentary rocks of the central Ompupa overlie rocks of the Kunene Complex (KC) (Bravo Silva et al., 2021; Carvalho et al., 1987; Carvalho and Simões, 1971; Escuder-Viruete et al., 2021a; Escuder-Viruete and Gumiel, 2021) and were intruded by ~ 1100 Ma mafic sills and dikes (Carvalho et al., 1987; Salminen et al., 2018). They are, therefore, Mesoproterozoic and are referred to as the Ompupa Group (Bravo Silva et al., 2021; Escuder-Viruete et al., 2021b; Labaredas et al., 2021). Similarly, the outliers located in the Cahama region are now interpreted as Mesoproterozoic (Escuder-Viruete and Gumiel, 2021) and referred to as the Cahama Formation. In the Iona region, suggested lateral correlatives of the ~ 1324 Ma Okapuka Formation of northwest Namibia (Kröner and Rojas-Agramonte, 2017) form the newly defined Iona Group, which might be Mesoproterozoic (Labaredas et al., 2021). In fact, the only correlative of the Namibian Damara Supergroup in southwest Angola may be the relatively small tabular units in cartographic continuity with Damara Supergroup rocks across the Cunene River (Labaredas et al., 2021). Although the Ompupa Group, Cahama Formation and Iona Group are thought to be Mesoproterozoic, they, as well as their underlying basement and cross-cutting granitoids, have been largely undated. This information is not only important for understanding the geological evolution of southwest Angola, but also because the Mesoproterozoic is a peculiar period of the geological record with rare ophiolites and passive margins, and abundant anorthosite and associated A-type granite magmatism (Roberts et al., 2023, and references therein), of which the Kunene Complex is the largest example in the world (Bybee et al., 2019; Milani et al., 2022; Rey-Moral et al., 2022).

Combined zircon U-Pb and Lu-Hf isotopic analyses have become increasingly popular in basin and crustal evolution studies (Belousova et al., 2010; Capaldi et al., 2021; Chu et al., 2016; Hall et al., 2018; Li et al., 2014; Roberts and Spencer, 2015; Sundell et al., 2019; Wu et al., 2020; Xu et al., 2013). Detrital zircons are commonly used to define maximum depositional ages for their hosts, as a sedimentary rock cannot be older than its youngest detrital grain(s). Additionally, these zircons can help identify sediment source terranes and trace sediment transport routes (Andersen et al., 2018; Dickinson and Gehrels, 2009; Gehrels, 2014; Zimmermann et al., 2015). On the other hand, the Hf isotopic composition of zircon traces crustal reworking and the addition of juvenile material from the depleted mantle (Andersen and Griffin, 2004; Belousova et al., 2010; Griffin et al., 2002). Combining U-Pb zircon ages and Hf isotopic compositions provides valuable information about the nature and composition of the continental crust that was formed during the main magmatic events within a region and helps to decipher their geodynamic setting (Chapman et al., 2017; Collins et al., 2011; Kemp et al., 2009; Kohanpour et al., 2019; Lloyd et al., 2016; Spencer et al., 2019; Sundell et al., 2019).

In this study, we present combined zircon U-Pb and Lu-Hf isotopic analyses from eight sedimentary samples from the Ompupa Group, Cahama Formation, and Iona Group, and six Paleo- and Mesoproterozoic igneous rocks from southwest Angola. Our aim is two-fold: to better constrain the depositional age of the Mesoproterozoic strata and determine their provenance; and to use the changing Lu-Hf isotopic composition of zircons in these strata as a proxy for the Archean to Mesoproterozoic crustal evolution of the southwest Angolan Shield.

2. Geological background

The study area is in southwest Angola, in the southwestern part of the Angolan Shield, where four main geotectonic zones have been identified (Carvalho et al., 2000; Jelsma et al., 2018; Rodrigues et al., 2021b): the Central Shield Zone in the northeast, the Cassinga Zone in the southeast, the Central Eburnean Zone in the west, and the Namibe Zone in the southwest. The Namibe Zone extends south to the Epupa Metamorphic Complex in northernmost Namibia. Further south, from west to east, are the Sesfontein, Kamanjab, Grootfontein, Tsumkwe, and Quangwadum inliers, forming the southwest margin of the AS (Fig. 1).

2.1. Archean to Paleoproterozoic basement

2.1.1. Southwest Angola

The Central Shield (CSZ) and Cassinga (CZ) zones form the Neoarchean nucleus of the AS. These two zones contain granite and granite-gneiss dated at 2682 ± 5 Ma to 2519 ± 5 Ma (with 2782 ± 6 Ma xenocrysts) in the CSZ (Jelsma et al., 2018), and at 2667 ± 15 Ma to 2568 ± 7 Ma in the CZ (Máximo et al., 2021a; Potti, 2021). Two presumably older but undated units occur in the CZ: the extensive Jamba Group and its underlying gneissic basement. The Jamba Group is a metavolcanic-sedimentary sequence intercalated with banded iron formation, metamorphosed at lower-greenschist facies conditions (Buzzi Marcos and Gutiérrez-Medina, 2021; Máximo et al., 2021a, 2021b and references therein). Intrusive into the Neoarchean nucleus, the Regional Granite is dated at 1974 ± 5 Ma to 1966 ± 3 Ma in the CSZ (Jelsma et al., 2018) and at 1982 ± 8 Ma to 1975 ± 10 Ma in the CZ (Gumiel et al., 2021; Máximo et al., 2021a). In the CSZ, the Regional Granite contains inherited zircons with ages of 2832–2816, 2670–2599, and 2539–2151 Ma (Jelsma et al., 2018).

The Regional Granite forms the bulk of the Central Eburnean Zone (CEZ, Fig. 1), where it is dominated by 2038 ± 28 Ma to 1947 ± 5 Ma biotite granitoids and coeval subvolcanic rocks (Galán, 2021; Gutiérrez-Medina et al., 2021; Jelsma et al., 2018; McCourt et al., 2013; Merino-Martínez and Goicoechea, 2021; Milani et al., 2022; Pereira et al., 2011). However, the CEZ may include fragments of older continental crust at depth, as revealed by zircon xenocrysts and inherited cores dated at 2263 ± 12,

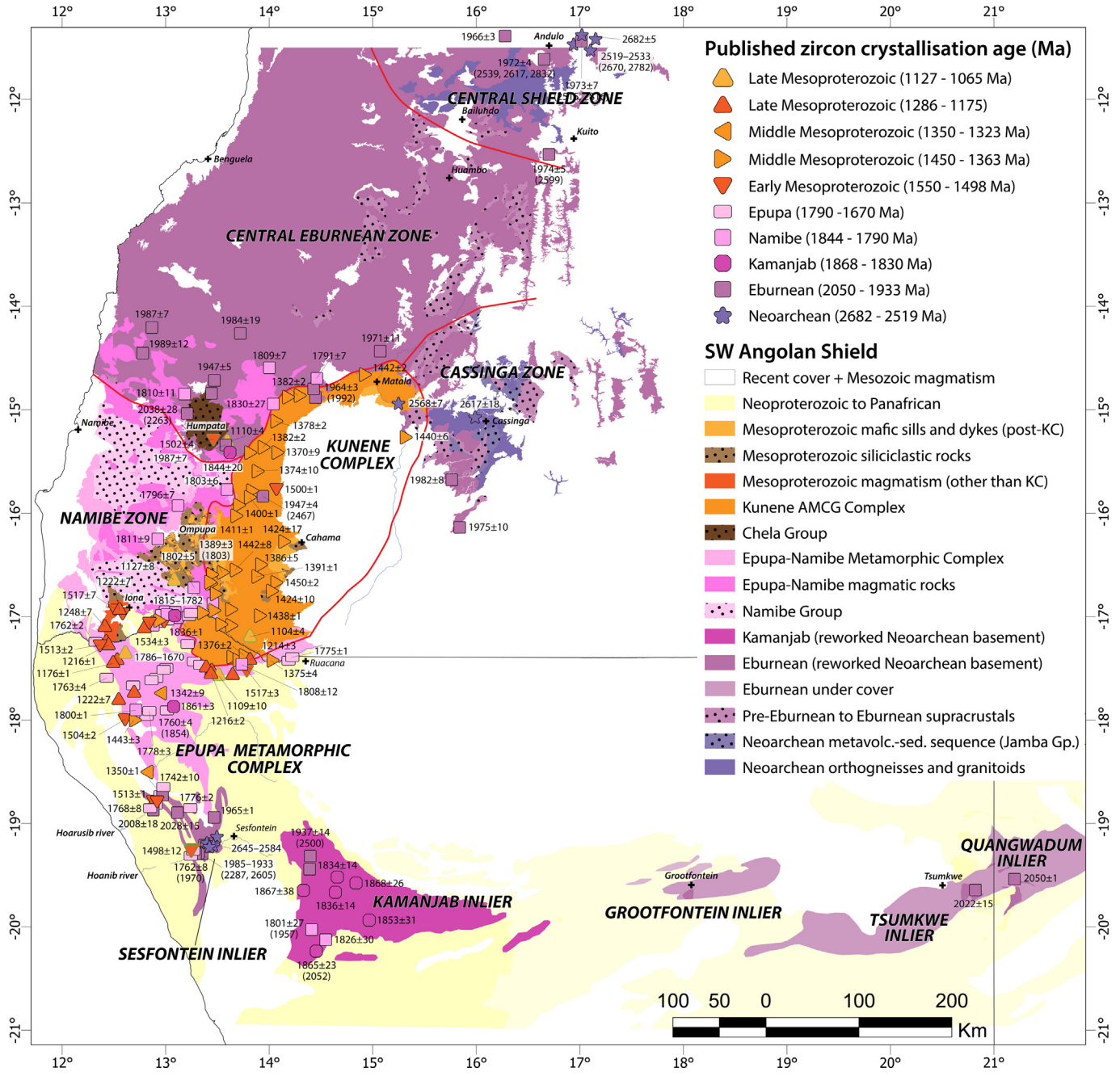

Fig. 1. Geological map showing the Precambrian geotectonic domains of the Angolan Shield of NW Namibia and SW Angola modified after Carvalho et al. (2000), Jelsma et al. (2018) and Rodrigues et al., (2021b) for Angola and after Lehmann et al. (2015, and reference therein) for Namibia. References for the reported published U-Pb crystallization ages are Franz et al. (1999), Seth (1999), Hoal et al. (2000), Littmann et al. (2000), Seth et al., (2003,2005), Singletary et al. (2003) Kröner et al., (2004,2010,2015), Mayer et al. (2004), Goscombe et al. (2005), Sanz (2005), Baxe (2007), Drüppel et al. (2007), Luft et al. (2011), Pereira et al. (2011), Ernst et al. (2013), Maier et al. (2013), McCourt et al. (2013), Kröner and Rojas-Agramonte (2017), Jelsma et al. (2018), Salminen et al. (2018), Bybee et al. (2019), Langa (2019), Lehmann et al. (2020), Brandt et al. (2021), Bravo-Silva et al. (2021), Escuder-Viruete et al., (2021b), Galán (2021), Gumiel et al. (2021); Gutiérrez-Medina et al. (2021); Máximo et al., (2021a); Merino-Martínez and Goicoechea (2021), Milani et al. (2022), Tshiningayamwe et al. (2022), Campeny et al. (2023), this study.

2467 ± 14 Ma and 2732 ± 43 Ma (Bravo Silva et al., 2021; McCourt et al., 2013; Milani et al., 2022). The 1844 ± 20 to 1791 ± 7 Ma shallow-level ultramafic to felsic magmatic rocks in the southern parts of the CEZ are coeval with the main magmatism in the abutting Namibe Zone (Bravo Silva et al., 2021; Campeny et al., 2023; Galán, 2021; McCourt et al., 2013; Milani et al., 2022; Pereira et al., 2011). This Paleoproterozoic crust is covered by the flat-lying metavolcanic-sedimentary sequence of the Chela Group (≤1798 ± 11 Ma to > 1502 ± 4 Ma; Ernst et al., 2013; McCourt et al., 2013; Pereira et al., 2011).

The Namibe Zone (NZ) is the youngest crustal domain of the southwestern AS in Angola (Merino-Martínez et al., 2021; Rodrigues et al., 2021b). The NZ is composed of a thick and spatially extensive package of volcano-sedimentary rocks, metamorphosed at greenschist facies conditions, known as the Namibe Group (Bravo Silva et al., 2021; Escuder-Viruete et al., 2021a; Labaredas et al., 2021) and formerly referred to as the Schist-Quartzite-Amphibolite Complex (Carvalho, 1981, 1984; Carvalho and Alves, 1993; Carvalho and Simões, 1971, 1972). The rocks of the Namibe Group grade into the upper amphibolite facies Namibe

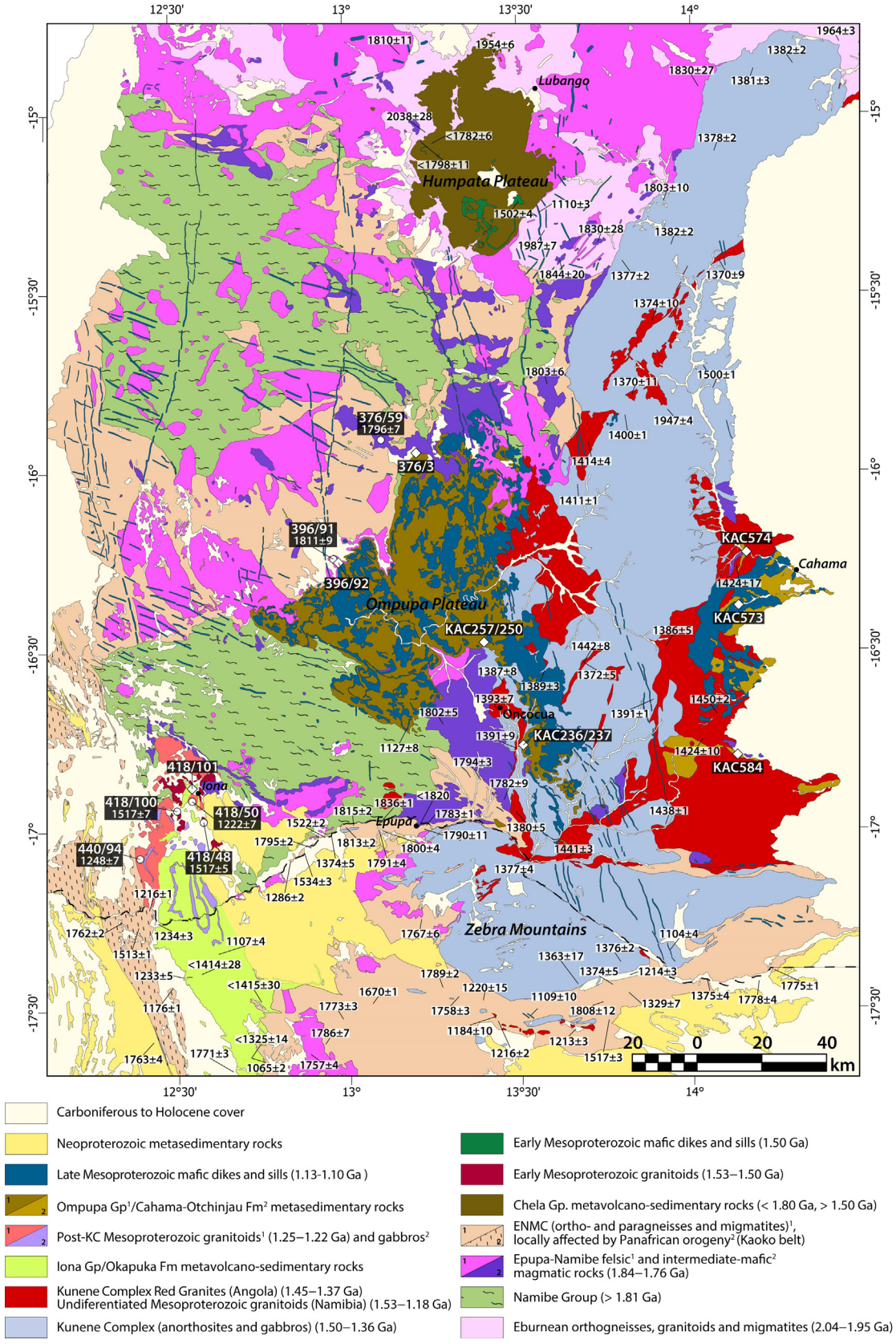

Fig. 2. New geological map for the study area based on the map of the Geological Survey of Namibia 1:250,000 and Kröner et al. (2010) for Namibia, and on the UTE-1 geological map at 1:500,000 scale of the Geological Institute of Angola (Rodrigues et al., 2021a). References for the reported published crystallization ages are the same as for Fig. 1.

Metamorphic Complex (NMC). The Namibe Group mainly consists of metapelite, metagreywacke, and felsic metavolcanoclastite, along with intercalated marble and amphibolite, whereas the NMC is made up of paragneiss, locally migmatitic, and related anatectic leucogranite, the latter containing xenoliths of siliciclastic rock, amphibolite, and marble (Bravo Silva et al., 2021; Carvalho and Simões, 1971, 1972; Escuder-Viruete et al., 2021a; Labaredas et al., 2021). The lithological association of the NMC, and its transitional contact with the Namibe Group, led several authors to suggest that the NMC formed as the result of progressive anatexis of the Namibe Group (Bravo Silva et al., 2021; Carvalho and Simões, 1971, 1972; Labaredas et al., 2021). Currently, the oldest rocks recognized in the NZ are mafic to felsic plutonics dating from 1803 ± 6 to 1782 ± 9 Ma (Escuder-Viruete et al., 2021b; Langa, 2019; Lehmann et al., 2020; Milani et al., 2022).

2.1.2. Northern Namibia

The NZ is juxtaposed with the Epupa Metamorphic Complex (EMC) of northwest Namibia (Fig. 1). The EMC is a composite Paleoproterozoic magmatic and metamorphic terrane, characterized by granite-gneiss and three polymetamorphosed supracrustal units (the Eyao, Epembe, and Orue units). Overall, the EMC consists of predominant migmatitic granite-gneiss with subordinate migmatitic metagreywacke, metapelite and metaquartzite, felsic and basic metavolcanite, and rare calc-silicate (Brandt et al., 2003, 2007, 2021; Brandt and Klemd, 2008; Kröner et al., 2010, 2015; Seth et al., 2003). The EMC was constructed by protracted felsic magmatism between 1861 ± 3 Ma and 1757 ± 4 Ma (Kröner et al., 2010, 2015; Seth et al., 2005), with a magmatic flare up around 1775 Ma, which might be coeval with migmatization (Kröner et al., 2010, 2015). More recently, Brandt et al. (2021) suggested a marginally younger anatectic event at ~ 1740–1720 Ma based on dates from zircon rims from the Eyao Unit. Limited younger Paleoproterozoic magmatism at 1670 ± 1 Ma was reported for an aplite dike in the northern part of the EMC (Kröner et al., 2010). The EMC supracrustal units' maximum depositional ages are ~ 1820 to ~ 1774 Ma for the Eyao Unit (Brandt et al., 2021; Kröner et al., 2015), ~1635 Ma for the Epembe Unit (Seth et al., 2003), and ~ 1671 Ma for the Orue Unit (Brandt et al., 2021; Seth et al., 2005), demonstrating that at least some of them were deposited after emplacement of the EMC granitoids. Several authors have noted the similarities and continuity of magmatic and metamorphic units of the NMC and EMC (Carvalho, 1969, 1972, 1984; Carvalho and Alves, 1993; Carvalho and Simões, 1972; Kröner et al., 2010, 2015). Consequently, we refer to them collectively as the Epupa–Namibe Metamorphic Complex (ENMC).

To the south of the EMC are other Paleoproterozoic inliers (Fig. 1), forming the southwestern margin of the AS, which include the Sesfontein, Kamanjab, Grootfontein and Tsumkwe inliers in Namibia and the Quangwadum inlier of NW Botswana (Franz et al., 1999; Hoal et al., 2000; Kleinhanns et al., 2013; Kröner et al., 2004; Luft et al., 2011; Sanz, 2005; Seth et al., 1998; Singletary et al., 2003). The Sesfontein Inlier contains the only known Archean rocks of the Namibian AS. These are granitoid-gneisses dated between 2645 ± 6 and 2584 ± 1 Ma (Seth et al., 1998; Franz et al., 1999; Seth, 1999), which are intruded by 2028 ± 15 Ma to 1933 ± 3 Ma Eburnean granitoids (Seth et al., 1998; Franz et al., 1999; Kröner et al., 2004; Luft et al., 2011; Seth, 1999). Similar Eburnean granitoid-gneiss has been reported in the Kamanjab, Grootfontein, Tsumkwe and Quangwadum inliers (Fig. 1; Hoal et al., 2000; Sanz, 2005; Singletary et al., 2003). In addition, the Kamanjab Inlier contains granite dated between 1868 ± 26 and 1801 ± 27 Ma, with inherited zircons between ~ 2052 and 1950 Ma and metamorphic zircon rims at 1778 ± 49 Ma (Kleinhanns et al., 2013; Sanz, 2005). The area between the Hoarusib and Hoanib rivers, near the Sesfontein Inlier, exhibits 1776 ± 2 Ma to 1684 ± 8 Ma granitoids (Goscombe et al., 2005; Kröner, 2005; Luft et al., 2011).

2.2. Mesoproterozoic magmatism, metamorphism and sedimentation

The Mesoproterozoic geological record of the AS is dominated by the formation of the largest anorthosite-mangerite-charnockite-granite (AMCG) complex in the world, the Kunene Complex (KC). The surface extent of the KC is ~ 18000 km^2 (Simpson, 1970); however, gravity modelling suggests it extends beneath Cenozoic sedimentary cover giving a total areal extent of ~ 42,500 km^2 (Rey-Moral et al., 2022). The KC anorthosites and granitoids (Red Granite Suite) were predominantly emplaced between 1442 ± 8 Ma and 1363 ± 17 Ma (Baxe, 2007; Bravo Silva et al., 2021; Bybee et al., 2019; Drüppel et al., 2007; Escuder-Viruete and Gumiel, 2021; Lehmann et al., 2020; Maier et al., 2013; Máximo et al., 2021a; Mayer et al., 2004; McCourt et al., 2013; Milani et al., 2022). However, Bybee et al. (2019) reported an older 1500 ± 1 Ma crystallization age for a pegmatoidal segregation within an anorthosite, suggesting that KC magmatism extended ~ 140 Myr.

There are slightly older/coeval Mesoproterozoic intrusions in the AS. These include poorly mapped A-type granite, located along the Kunene River and between the Hoarusib and Hoanib rivers, which intruded the ENMC between 1534 ± 3 Ma and 1498 ± 12 Ma (Kröner and Rojas-Agramonte, 2017). There are also mafic sills emplaced into the Chela Group of the Humpata Plateau at 1502 ± 4 Ma (Ernst et al., 2013). Younger Mesoproterozoic intrusions are restricted to the ENMC in northern Namibia and include A-type granite, gabbro-peridotite, nepheline syenite and carbonatite dated from 1286 ± 2 Ma to 1176 ± 1 Ma, with most ages ranging between 1234 ± 3 and 1214 ± 3 Ma (Kröner and Rojas-Agramonte, 2017; Littmann et al., 2000; Maier et al., 2013; Simon et al., 2017).

Mesoproterozoic metamorphism is so far exclusively reported for the ENMC in northern Namibia. An ultra-high-temperature granulite facies metamorphic event was dated at ~ 1533–1511 M a in the Epembe Unit (Brandt et al., 2003, 2007, 2021; Seth et al., 2003), making it broadly coeval with granulite facies contact metamorphism in the Eyao Unit, although they are not considered to be related (Brandt et al., 2021). A later anatectic upper-amphibolite facies metamorphic event affected the Orue Unit at ~ 1340–1320 Ma (Brandt et al., 2021; Seth et al., 2003).

The siliciclastic rocks of the Ompupa and Iona groups, and the Cahama Formation, unconformably overlie the Namibe Zone Paleoproterozoic basement and the KC (Bravo Silva et al., 2021; Escuder-Viruete et al., 2021b; Escuder-Viruete and Gumiel, 2021; Labaredas et al., 2021). The supracrustal rocks of the Okapuka Formation are ~ 1324 Ma (Kröner and Rojas-Agramonte, 2017) and are in spatial continuity with the Iona Group (Carvalho and Alves, 1993; Kröner and Correia, 1980; Labaredas et al., 2021). Regionally extensive undeformed mafic dikes and sills dated between 1127 ± 8 and 1104 ± 4 Ma (Ernst et al., 2013; Salminen et al., 2018), along with a felsic sill dated at 1065 ± 2 Ma (Kröner and Rojas-Agramonte, 2017), mark the end of Mesoproterozoic magmatism in the southwest AS.

3. Samples and analytical methods

3.1. Sampling

In this study, eight samples of siliciclastic rocks representing the Mesoproterozoic strata of southwest Angola and six igneous samples previously mapped as Regional Granite were collected for U-Pb and Lu-Hf zircon analysis. The location of the samples is

shown in Fig. 2. Additionally, field photos of the samples are provided as Supplementary Data (Supplementary Data, Figures S1 and S2).

Siliciclastic samples 376/3, 396/92, KAC257/250, and KAC236/237 are from the Ompupa Group. Samples 376/3 (-15.94624, 13.21427) and 396/92 (-16.25005, 12.97783) are microconglomeratic lithic arkose that overlies granitoids in the northwestern part of the Ompupa Plateau. Samples KAC257/250 (-16.48470, 13.40196) and KAC236/237 (-16.76645, 13.49902) are fine-grained lithic arkose and medium-grained quartz arenite that overlie KC anorthosite in the central and southern parts of the Ompupa plateau, respectively. The unconformable contact between the arkose of sample 396/92 and the underlying leucogranite (396/91; −16.25005, 12.97783) is observed, whereas the contact between the arkose of sample 376/3 and the underlying granodiorite (376/59; −15.90847, 13.09664) is inferred as it is covered by slope deposits. The contact between the sedimentary strata sampled as KAC257/250 and KAC236/237 and the KC anorthosite is inferred from a break in topographic slope. The latter two samples were collected within the basal first 100 m of the sedimentary sequence.

Samples KAC573, KAC574 and KAC584 are representative of the Cahama Formation. Sample KAC573 (-16.37900, 14.13451) is a fine-grained lithic arenite collected from an area of extensive late Mesoproterozoic mafic units (Fig. 2). Sample KAC574 (-16.22390, 14.15957) is a poorly sorted fine- to coarse-grained quartz-arenite overlying Red Granite collected from the basal 20 m of the sedimentary sequence. Sample KAC584 (-16.79269, 14.12956) is a polymictic conglomerate from ~ 400 m (effective distance) above an inferred concordant contact with underlying Cahama Formation felsic volcanic rocks.

Sample 418/101 (-16.884293, 12.56362) is a medium- to coarse-grained quartz-arenite from the Iona Group. At this location, the Iona Group is intruded by rhyolite porphyries (418/50; −16.92121, 12.54978). Additionally, we collected three granitoids from the Iona region that lack geochronological constraints. Samples 418/48 (-16.97479, 12.58054) and 418/100 (-16.93884, 12.50911) are alkali-feldspar granites (Fig. 2). Sample 440/94 (-17.08704, 12.40840) represents an alkali feldspar porphyritic granite-gneiss. These so far undated granitoids were typically mapped as part of the Regional Granite and interpreted to be intrusive into the Iona Group (Carvalho, 1981; Carvalho and Alves, 1993; Serv. Geol. Minas Angola, 1961).

3.2. Zircon separation and cathodoluminescence imaging

Samples were crushed in a jaw crusher, milled, and sieved to < 500 μm, followed by water-washing in a Wilfley table to produce a heavy mineral concentrate. The resulting heavy fraction was briefly washed in acetone and allowed to dry. Ferromagnetic minerals were subsequently removed using a hand-magnet. Finally, zircons were randomly hand-picked under a binocular microscope, mounted in epoxy, and polished to expose the interior of the grains. Cathodoluminescence (CL) images were obtained to reveal the internal structure of the zircons and select spots for U-Pb and Lu-Hf analyses. CL images of zircons from the metasedimentary samples were acquired using a Tescan scanning electron microscope at the Spectrum Analytical Facility, University of Johannesburg (South Africa), whereas zircons from the igneous samples were imaged using a Quanta 250 FEI scanning electron microscope equipped with an XMAX CL detector at the Geochronological Research Center of the University of São Paulo (CPGeo, Brazil).

3.3. U-pb analyses

U-Pb zircon analyses of the metasedimentary samples were performed at the Spectrum Analytical Facility at the University of Johannesburg, using a 193 nm ArF RESOlution SE Excimer laser ablation system coupled to a Thermo iCAP-RQ quadrupole-based inductively coupled plasma mass spectrometer (Q-ICPMS), except for samples KAC573, KAC574, and KAC584, which were analysed using a Nu Plasma II multi-collector inductively coupled mass spectrometer (MC-ICPMS), following the procedures by Andersen et al. (2009) and Vorster (2013). The U-Pb zircon analyses of the igneous samples were conducted at the High-Resolution Geochronology Laboratory (GeoLab-SHRIMP) of the University of São Paulo using a Sensitive High-Resolution Ion Microprobe (SHRIMP-IIe), and analytical routines described by Williams (1998). Detailed information on the U-Pb analytical procedures is provided as Supplementary Data A. U-Pb zircon data for our samples and the secondary standards (CDQGNG and TEMORA-2) are provided in Supplementary Data (Tables S1 to S5).

U-Pb ages were calculated using IsoplotR (Vermeesch, 2018). Wetherill and Tera–Wasserburg diagrams were generated using Isoplot v.4.15 (Ludwig, 2012). The uncertainties of the U-Pb ages reported in the text are at a 2σ level. The detrital zircon U-Pb ages are reported as Concordia ages (Ludwig, 1998; Vermeesch, 2021a). The detrital zircon data were filtered and only "concordant" analyses meeting the following criteria were used for age plots and discussion: +10 to −5% discordance, isotopic ratio uncertainty < 10 % (2σ), and $^{206}Pb/^{204}Pb$ > 1000. Maximum depositional ages (MDA) were calculated using the maximum likelihood age (MLA) algorithm of Vermeesch (2021b). The MLA statistically resolves the limitations and biases of the different MDA approaches, which tend to shift MDAs towards either younger or older ages (see Coutts et al., 2019; Vermeesch, 2021b for a thorough review). The age of youngest single concordant grain (YSG) and of the weighted mean of the youngest cluster of zircon ages that overlap within uncertainties at 1σ (YC1σ 2 +) and 2σ (YC2σ 3 +) are also reported in Table 1. The MDAs determined with the MLA algorithm are within uncertainty of the values obtained by the YC1σ 2 + and YC2σ 3 +. When compared with the age provided by the YSG, the difference tends to increase as the number of detrital zircons in the youngest cluster increases, consistent with the findings of Vermeesch (2021b and references therein). Kernel density estimation (KDE; 20 Myr set as kernel bandwidth and as binwidth) and cumulative distribution function (CDF) plots were generated using Density Plotter (Vermeesch, 2012) and IsoplotR (Vermeesch, 2018), respectively. The detrital zircon U-Pb age distributions were compared with potential source rocks using the Kolmogorov-Smirnov (K-S) test and multidimensional scaling (MDS) analysis. The K-S test was performed using the Excel macro "K-S test" (Guynn and Gehrels, 2010). P-values less than 0.05 indicate significant differences in the age distributions at a 95 % confidence level (Guynn and Gehrels, 2010). The dissimilarity matrix of the K-S test P-values is provided in Supplementary Data (Table S6). The MDS plot was generated using DZmds v1.10 (Saylor et al., 2018) and used the K-S test as dissimilarity measure, along with a metric-square stress criterion. The obtained stress value of 0.083 indicates a good fit and reliable transformation of dissimilarities into 3D space (Supplementary Data, Figure S3).

3.4. Lu-Hf analyses

Lu-Hf analyses were conducted at the Spectrum Analytical Facility at the University of Johannesburg, using the 193 nm ArF

Table 1
Detrital zircon U-Pb maximum depositional age estimates in Mesoproterozoic strata of SW Angolan Shield. U-Pb crystallization ages for the underlying igneous basement and crosscutting intrusive rocks are also provided.

Unit	Sample	Maximum depositional age estimates (Ma ± 2σ)				Crystallization age (Ma ± 2σ)	
		YSG	YC1σ (2 +)	YC2σ (3 +)	MLA	Underlying	Crosscutting
Ompupa Group	376/3	1294.7 ± 33.9	1314.3 ± 8.4 (n = 17) MSWD = 0.30, p = 1.00	1334.6 ± 5.2 (n = 50) MSWD = 1.2, p = 0.16	1324.1 ± 9.8	1810.8 ± 9.3	1127 ± 8[*1]
	396/92	1302.5 ± 27.9	1318 ± 8 (n = 9) MSWD = 0.33, p = 0.96	1335 ± 4.7 (n = 26) MSWD = 1.4, p = 0.09	1333.8 ± 8.3	1796.3 ± 7	
	KAC257/250	1174.7 ± 20.1	1176 ± 17 (n = 2) MSWD = 0.06, p = 0.80	1189 ± 56 (n = 3) MSWD = 3.5, p = 0.03	1184.2 ± 22.6 1221.9 ± 18.9 (excl. 2 youngest grains)	1389 ± 3[*2]	
	KAC236/237	1212.8 ± 23.9	1224 ± 17 (n = 2) MSWD = 1.8, p = 0.18	1238 ± 11 (n = 5) MSWD = 2.0, p = 0.09	1229.9 ± 23.2	1391 ± 9[*3]	
Cahama Formation	KAC573	1214.7 ± 13.3	1321 ± 11 (n = 2) MSWD = 1.4, p = 0.23	1332 ± 38 (n = 3) MSWD = 4.8, p = 0.01	1214.7 ± 13.3 1321.5 ± 11.6 (excl. youngest grain)	1424 ± 17[*4]	1127 ± 8 (?)
	KAC574	1472.7 ± 22	1482 ± 13 (n = 2) MSWD = 1.04, p = 0.31	1489 ± 10 (n = 3) MSWD = 2.1, p = 0.13	1482.2 ± 23		
	KAC584	1747.9 ± 10.6	1757 ± 14 (n = 2) MSWD = 1.3, p = 0.25	1769.6 ± 8.3 (n = 4) MSWD = 2.0, p = 0.11	1769.6 ± 9.4	1424 ± 10[*4]	
Iona Group	418/101	1310.9 ± 17.5	1311 ± 10 (n = 5) MSWD = 0.33, p = 0.86	1329 ± 14 (n = 11) MSWD = 0.65, p = 0.78	1322.5 ± 13.4	1516.9 ± 5.3	1222.2 ± 6.5

Methods for maximum depositional ages estimation: YSG - youngest single concordant grain; YC1σ (2 +) - youngest cluster of ≥ 2 grains overlapping at ± 1σ uncertainty; YC2σ - youngest cluster of ≥ 3 grains overlapping at ± 2σ uncertainty; MLA - maximum likelihood age.
"*1–4": literature data from Salminen et al. (2018), Bybee et al. (2019), Lehmann et al. (2020) and Escuder-Viruete and Gumiel (2021). "(?)": estimated crystallization age.

RESOlution SE Excimer laser ablation system coupled to the Nu Plasma II multi-collector ICPMS. Detailed information on the Lu-Hf analytical procedures is provided as Supplementary Data A. Lu-Hf zircon data for our samples and the secondary standards (TEMORA-2, Mud Tank, and LV-11 after Heinonen et al., 2010; Woodhead and Hergt, 2005) are provided in Supplementary Data (Tables S7 and S8).

Initial $^{176}Hf/^{177}Hf$ values are expressed as $\varepsilon Hf_{(i)}$, calculated using a ^{176}Lu decay constant of 1.867×10^{-11} y^{-1} (Söderlund et al., 2004) and present-day chondritic uniform reservoir (CHUR) values of $^{176}Lu/^{177}Hf_{CHUR} = 0.0336$ and $^{176}Hf/^{177}Hf_{CHUR} = 0.282785$ (Bouvier et al., 2008). For detrital zircons, $\varepsilon Hf_{(i)}$ values were calculated using the apparent age of the individual U-Pb measurement. In the case of igneous zircons, $\varepsilon Hf_{(i)}$ values were calculated using the magmatic crystallization age derived from the zircon U-Pb dataset, except for inherited cores or xenocrysts, which were calculated using the apparent age of the individual U-Pb measurement (Vervoort and Kemp, 2016). The calculation of two-stage Hf model ages (TDM_2) was performed using the bulk continental crust $^{176}Lu/^{177}Hf_{BCC}$ value of 0.0116 (Rudnick and Gao, 2014) and a modified version of the depleted mantle model of Griffin et al. (2000), with present-day values of $^{176}Lu/^{177}Hf_{DM} = 0.0388$ and $^{176}Hf/^{177}Hf_{DM} = 0.28325$ ($\varepsilon Hf = +16.4$) (Andersen et al., 2011). Given the strong dependency of TDM_2 ages on the selected model parameters, their use in this study is restricted to fingerprinting and comparison purposes. In this regard, any model chosen would be equally effective provided it was consistently implemented (Andersen et al., 2018, 2016a, 2016b). Lu-Hf data from the literature reported in this study were recalculated using the parameters mentioned above. Nd-TDM ages from the literature were also recalculated assuming a two-stage evolution, considering a linear isotopic growth of the depleted mantle starting with an εNd value of + 10 at present. The following parameters were used for the recalculation: $^{143}Nd/^{144}Nd_{DM} = 0.51315$ and $^{147}Sm/^{144}Nd_{DM} = 0.2137$ for the depleted mantle (Peucat et al., 1989) and $^{147}Sm/^{144}Nd_{BCC} = 0.1180$ for the bulk continental crust (Rudnick and Gao, 2014). HafniumPlotter v1.70 (Sundell et al., 2019) was used to generate 2D KDE plots of the U-Pb ages versus $\varepsilon Hf_{(i)}$ values for our study and compiled literature data (20 Myr and 1 εHf unit were set as kernel bandwidths).

4. Results

4.1. U-pb and Lu-Hf isotopes

4.1.1. Igneous rocks

376/59 and 376/91: granodiorite and leucogranite

Zircons are euhedral to subhedral, ranging from stubby and nearly equidimensional to elongated prismatic forms with aspect ratios up to 1:3 and between 100 and 200 μm in length. Zircons in CL exhibit well-developed oscillatory zoning, locally containing inherited cores, and, more rarely, striped zoning. Zircons in sample 396/91 display common fracturing and dark (high-U), mottled, metamict rims and/or alteration fronts, which locally results in the near pervasive modification of the crystals (Fig. 3).

Twelve U-Pb analyses (on 11 zircons) from sample 376/59 (Fig. 4A) give an upper intercept age of 1801.4 ± 9.2 Ma (MSWD = 0.80, ρ = 0.63) and a lower intercept of 507 ± 120 Ma. The upper intercept age is identical within uncertainty to the mean $^{207}Pb/^{206}Pb$ age of 1796.3 ± 7.0 Ma (MSWD = 1.1, ρ = 0.36, n = 10), interpreted as the crystallization age of the granodiorite. The Lu-Hf analyses of 16 zircons show $\varepsilon Hf_{(i)}$ values ranging from −2.1 to 0 (average = −1.2 ± 0.7) and TDM_2 ages between 2451 and 2342 Ma (average = 2405 ± 36 Ma) (Fig. 5, Supplementary Data Table S7). Two analyses have lower $\varepsilon Hf_{(i)}$ values of −5.6 and −4.7 with TDM_2 ages of 2639 and 2591 Ma, respectively, and are potentially small inherited cores.

Twelve U-Pb analyses (on 12 zircons) from sample 396/91 (Fig. 4B) give an upper intercept age of 1814.2 ± 9.3 Ma (MSWD = 0.28, ρ = 0.99). This age is identical within uncertainty to the concordia age of 1810.8 ± 9.3 Ma (MSWD = 0.55, ρ = 0.90,

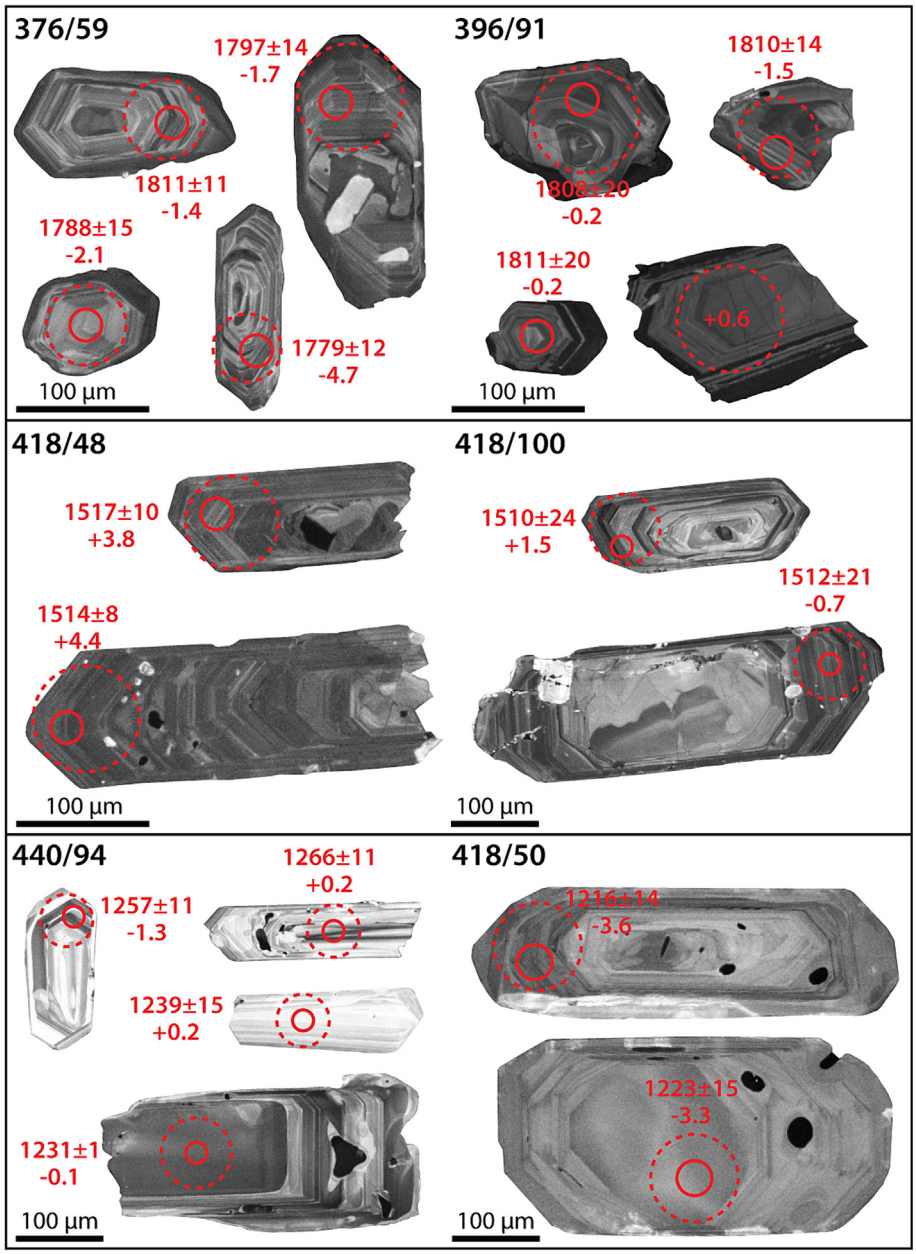

Fig. 3. Representative cathodoluminescence (CL) images of zircon grains from the studied igneous samples. Also shown are laser spot positions for U–Pb dating (solid circles) and Hf isotope analyses (dashed circles), as well as U-Pb ages (Ma) and $\varepsilon Hf_{(i)}$ values for each spot. U-Pb age errors are 1 sigma.

n = 7), interpreted as the crystallization age of the leucogranite. The $\varepsilon Hf_{(i)}$ values of 16 zircons range from −2.3 to + 1.5 (average = −0.3 ± 1.1), with TDM_2 ages between 2475 and 2272 Ma (average = 2371 ± 57 Ma). One analysis has an $\varepsilon Hf_{(i)}$ value of −7.1 and a TDM_2 age of 2727 Ma, and is potentially an inherited core (Fig. 5, Supplementary Data Table S7).

418/48 and 418/100: alkali-feldspar granites.

Zircons predominantly form long euhedral prisms, ranging between 150 and 500 µm in length (average of 250 µm), and have aspect ratios of 1:2 to 1:4. Zircons in CL exhibit well-developed oscillatory zoning, with some zircon showing convolute-zoned or dark (high-U), mottled, metamict cores. Fractures are common and zircons typically exhibit bright or dark luminescence inclusions (Fig. 3).

Sixteen U-Pb analyses (on 16 zircons) from sample 418/48 (Fig. 4C) give an upper intercept age of 1525.8 ± 9.1 Ma (MSWD = 1.3, ρ = 0.19) and a lower intercept age of 552 ± 88 Ma. The upper intercept age is identical within uncertainty to the concordia age of 1516.9 ± 5.3 Ma (MSWD = 0.89, ρ = 0.58, n = 9), interpreted as the crystallization age of the alkali-feldspar-rich granite. The $\varepsilon Hf_{(i)}$ values of 14 zircons range from + 1.9 to + 4.1 (average = +3.2 ± 0.7), with TDM_2 ages between 2019 and 1897 Ma (Fig. 5, Supplementary Data Table S7).

Sixteen U-Pb analyses (on 12 zircons) from sample 418/100 (Fig. 4D) provide an upper intercept age of 1521 ± 11 Ma (MSWD = 0.38, ρ = 0.98). This age is identical within uncertainty to the concordia age of 1517.1 ± 7.0 Ma (MSWD = 1.2, ρ = 0.27, n = 9), interpreted as the crystallization age of the leucogranite.

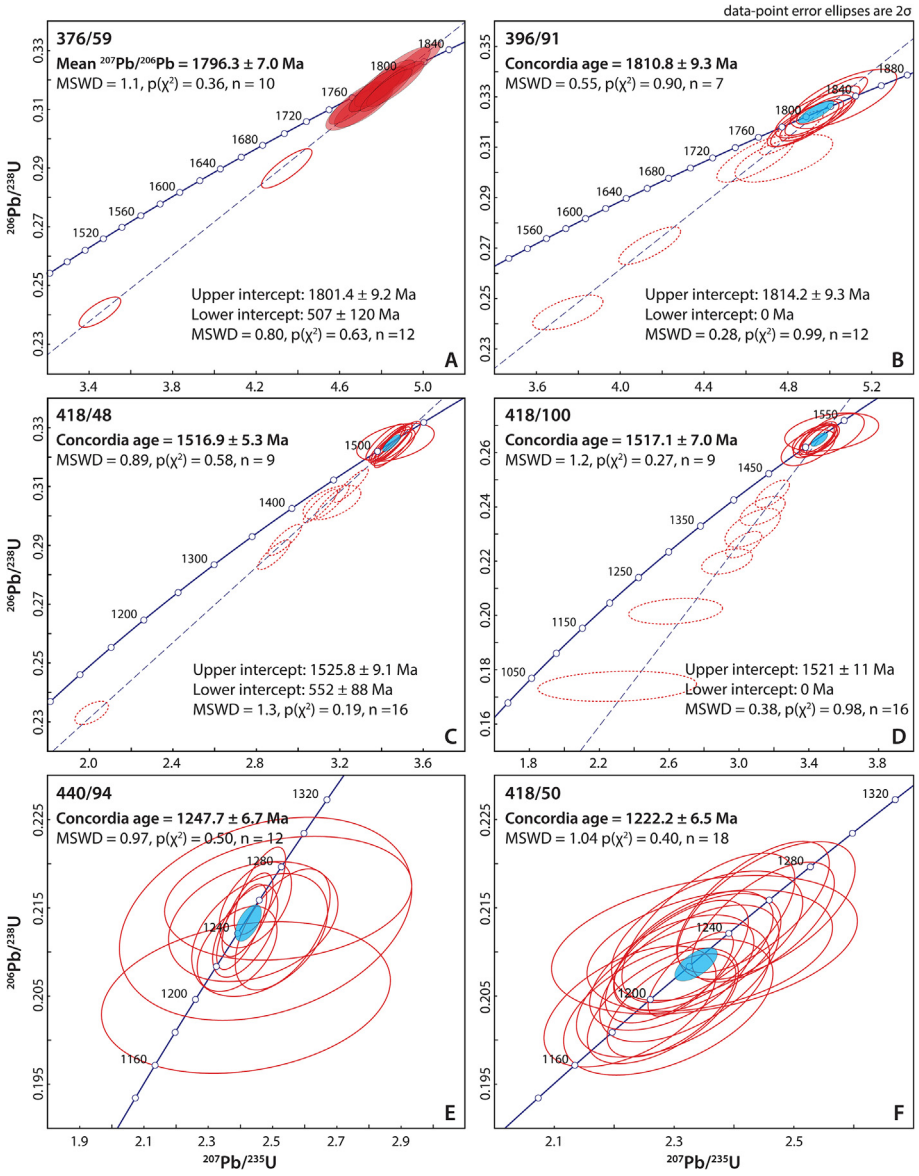

Fig. 4. Concordia diagrams for the studied igneous samples: A) 376/59 (granodiorite), B) 396/91 (leucogranite), C) 418/48 (alkali-feldspar granite), D) 418/100 (alkali-feldspar granite), E) 440/94 (alkali-feldspar porphyritic granite-gneiss), F) 418/50 (rhyolite porphyry). Dashed ellipses were not considered for Concordia age calculation but were used for upper intercept age calculation. Discordia lines for samples 396/91 and 418/100 are anchored at the origin of the diagram (0 Ma).

The $\varepsilon Hf_{(i)}$ values of 18 zircons range from −0.9 to + 2.6 (average = +1.1 ± 1.0) and with TDM_2 ages between 2167 and 1979 Ma (Fig. 5, Supplementary Data Table S7).

440/94: alkali feldspar porphyritic granite-gneiss.

Zircons mainly form long euhedral prisms, varying in length from 150 to 350 μm (average 200 μm), with aspect ratios typically around 1:3, but ranging from 1:2 to 1:6. Zircons in CL generally show clear oscillatory to striped zoning, although some grains show a gradational increase in luminescence, and accompanying decrease in U, Th, and Pb contents (Supplementary Data Table S4), which we attribute to metamorphic recrystallization. Despite this, there are no discernible differences in the U-Pb or Lu-Hf isotopic composition among the analysed zircons, except for a higher age uncertainty in those with enhanced luminescence. Low-luminescence inclusions are commonly observed (Fig. 3).

Twelve U-Pb analyses (on 12 zircons) give a concordia age of 1247.7 ± 6.7 Ma (MSWD = 0.97, ρ = 0.50), interpreted as the crystallization age of the granite-gneiss (Fig. 4E). The $\varepsilon Hf_{(i)}$ values of 23 zircons range from −2.0 to + 0.6 (average = −0.5 ± 0.8), with TDM_2 ages between 2033 and 1890 Ma. One analysis yields a lower $\varepsilon Hf_{(i)}$ value of −3.8 and a TDM_2 age of 2131 Ma (Fig. 5, Supplementary Data Table S7).

418/50: rhyolite porphyry.

Zircons form elongated euhedral to subhedral prisms, with lengths ranging between 350 and 700 μm (average 500 μm) and aspect ratios typically around 1:4 (ranging from 1:2 to 1:6). Zircons in CL show well-defined oscillatory zoning and abundant low-luminescence inclusions.

Eighteen U-Pb analyses (on 17 zircons) define a concordia age of 1222.2 ± 6.5 Ma (MSWD = 1.04, ρ = 0.40), interpreted as the crystallization age of the rhyolite porphyry (Fig. 4F). The $\varepsilon Hf_{(i)}$ values of 18 zircons range from −4.6 to −2.8 (average = −3.6 ± 0.4), with TDM_2 ages between 2158 and 2058 Ma (Fig. 5, Supplementary Data Table S7).

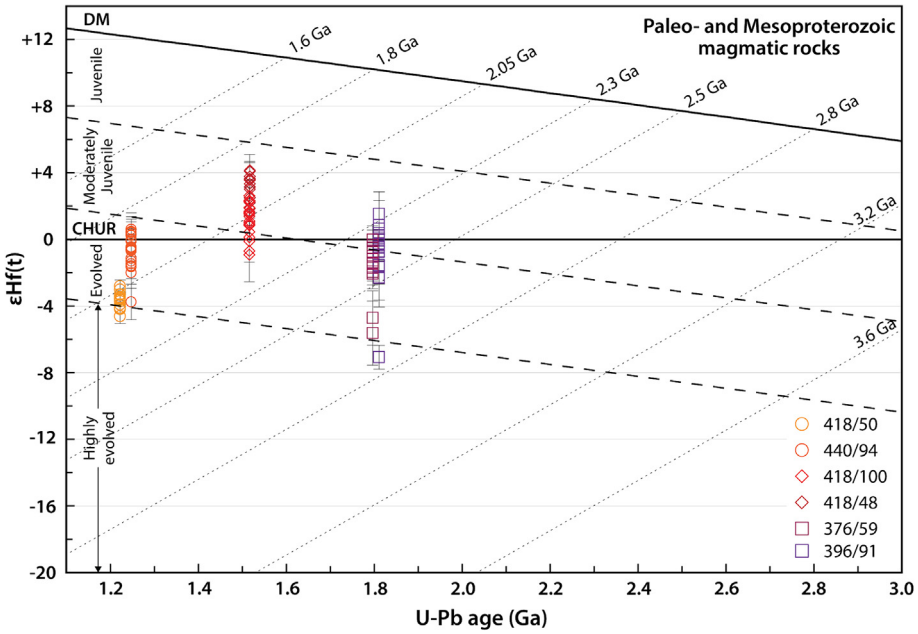

Fig. 5. U-Pb age versus $\varepsilon Hf_{(i)}$ diagram for igneous zircons from the studied igneous rock samples. Based on a modified version from Reimann et al. (2010) and Sundell et al. (2019), we classify differences between the TDM_2 age and the zircon's crystallization age of less than 300 Myr (< ~5 εHf units) of the depleted mantle as juvenile, 300 to 600 Myr as moderately juvenile (~5 to 10 εHf units), 600 to 900 Myr as evolved, and greater than 900 Myr as "highly evolved" (>~15 εHf units).

4.1.2. Sedimentary rocks

A total of 805 U-Pb isotopic analyses were performed on 797 detrital zircon grains from eight siliciclastic samples. Among these, 673 analyses yielded concordant U-Pb ages. Additionally, 295 concordant zircons representative of each of the main U-Pb age groups were selected for Lu-Hf isotope analysis. Most of the analysed zircons have $^{232}Th/^{238}U$ ratios > 0.1, consistent with an igneous origin (Hoskin, 2003; Hoskin and Black, 2000; Rubatto, 2017; Supplementary Data, Table S9).

Fig. 6 presents representative CL images of the examined detrital zircon grains. Zircons range in shape from nearly equidimensional to elongated prisms. In conglomeratic samples (376/3, 396/2, and KAC584), most zircons are angular to subangular, with subordinate subrounded grains, and with lengths between ~ 100 and 250 μm (most are > 150 μm). In arenitic samples (KAC257/250, KAC236/237, KAC573, KAC574, 418/101), most zircons are subrounded to rounded, with subordinate subangular to angular forms. Zircons in these samples are generally < 150 μm in length. Fine-grained samples KAC257/250 and KAC573 have a higher proportion of grains between 50 and 100 μm in length. An exception is sample KAC574, as it contains coarser-grained zircons, typically > 150 μm and up to 300 μm in length. Most zircons in CL exhibit growth zoning textures characteristic of magmatic zircons, marked by oscillatory or fine to broad striped zoning, and less commonly, sector zoning. A few grains are homogeneous and lack primary zoning, whereas others show bright rims of variable widths that truncate magmatic growth zoning, indicating post-magmatic crystallization, alteration or a metamorphic origin. Considering the low metamorphic grade of the studied sedimentary samples, we infer that these later features occurred before their deposition.

For the entire U-Pb and Lu-Hf dataset, Fig. 7A is a KDE plot illustrating the U-Pb detrital zircon age distribution and Fig. 7B shows the U-Pb detrital zircon age vs $\varepsilon Hf_{(i)}$ value. For each sample, Fig. 8 displays the U-Pb isotopic data in KDE and CDF plots and Fig. 9 the U-Pb zircon age versus $\varepsilon Hf_{(i)}$. U-Pb isotopic data in Tera–Wasserburg diagrams are presented in Supplementary Data (Figure S4).

The KDE plot indicates that the dataset can be broadly divided into four distinct groups, with U-Pb ages ranging from ~ 3.45 to 1.18 Ga (Fig. 7A).

The oldest group, comprising 8 % of the dataset, is characterized by scattered early Siderian to Archean ages (~3.45 to 2.30 Ga). It shows broad peaks at approximately ~ 2.72, 2.61, and 2.45 Ga. The $\varepsilon Hf_{(i)}$ values range from −8.9 to + 3.7, with TDM_2 ages between 3.88 and 2.80 Ga. There is an overall trend of decreasing $\varepsilon Hf_{(i)}$ values with younger U-Pb ages.

The second group, known as the Eburnean group, represents 22 % of the dataset and consists of Paleoproterozoic ages ranging from late Rhyacian to early Orosirian. This group is characterized by a prominent peak centred around 1.96 Ga, followed by a long tail extending towards older ages up to ~ 2.18 Ga, with a significant cluster at ~ 2.02 Ga. Most Eburnean zircons (n = 52; 84 %) exhibit markedly negative $\varepsilon Hf_{(i)}$ ranging from −12.8 to −4.5 (average = −8.5 ± 2.2) and TDM_2 ages between 3.12 and 2.73 Ga (average = 2.94 ± 0.10 Ga). The Eburnean zircons broadly align with the crustal evolution trend defined by the Siderian to Archean zircons. However, there is a small group of zircons (n = 10; 14 %) with ages ~ 2.1 Ga (n = 2) and ~ 1.94–1.91 Ga (n = 8) that deviate from this trend and exhibit sub-chondritic $\varepsilon Hf_{(i)}$ (average = −1.4 ± 1.7) and lower TDM_2 ages (average = 2.56 ± 0.09 Ga).

The third group of zircons, accounting for 33 % of the dataset, are Paleoproterozoic with late Orosirian to Statherian ages. This group is characterized by three age peaks at ~ 1.86, 1.81, and 1.77 Ga. This group is referred to as Kamanjab-–Namibe–Epupa (K-N-E) after the main regions where these ages are found (see Fig. 1 and Section 2). $\varepsilon Hf_{(i)}$ typically ranges between −5.5 and + 4.2 (average = −1.1 ± 1.9) with TDM_2 ages from 2.66 to 2.11 Ma (2.40 ± 0.12 Ma). This range in $\varepsilon Hf_{(i)}$ is, in general, significantly more radiogenic than the second group. However, four zircons from the third group plot along a crustal evolution trend defined by the Eburnean and older zircons and have $\varepsilon Hf_{(i)}$ values between −12.0 and −8.6 with TDM_2 ages between 3.00 and 2.84 Ga.

The fourth and youngest group of zircons, representing 37 % of the dataset, consists of Mesoproterozoic ages and displays two

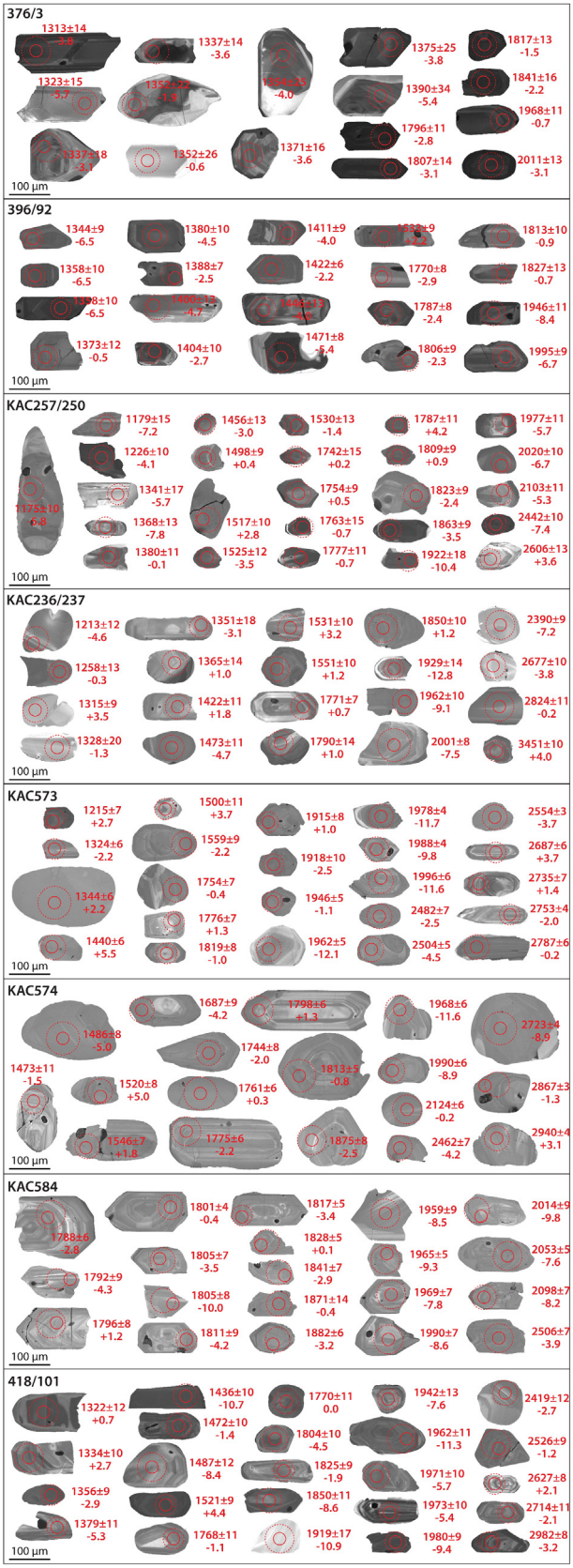

Fig. 6. Representative cathodoluminescence (CL) images of zircon grains from the studied detrital samples. Also shown are laser spot positions for U–Pb dating (solid circles) and Hf isotope analyses (dashed circles), as well as U-Pb ages (Ma) and $\varepsilon Hf_{(i)}$ values for each spot. U-Pb age uncertainties are 1 sigma.

prominent peaks at ~ 1.38 and ~ 1.35 Ga (early Ectasian). This group is followed by two smaller peaks centred at ~ 1.53 and ~ 1.48 Ga (early Calymmian), along with a smaller and younger population at ~ 1.23–1.18 Ga. In general, the Mesoproterozoic zircons exhibit a broad range of $\varepsilon Hf_{(i)}$ ranging from −8.4 to + 5.6 (average = −1.7 ± 3.2) with TDM_2 ages from 2.54 to 1.73 Ma (average = 2.11 ± 0.16 Ma). The ~ 1.56–1.50 Ga zircons display distinctly more juvenile $\varepsilon Hf_{(i)}$ than the crustal evolution trend defined by the K-N-E zircons. A similar pattern is also locally observed in the rest of the Mesoproterozoic ages. There is also a group of four zircons with ages ~ 1.56 (n = 1), ~1.49 (n = 1) and ~ 1.44 (n = 2) that exhibit significantly more negative $\varepsilon Hf_{(i)}$ (-15.6 to −8.4) and which are compatible with the crustal evolution trend defined by the Eburnean and older zircons.

A detailed sample-by-sample description of the U-Pb and Lu-Hf results of the sedimentary samples is provided in Supplementary Data B.

5. Discussion

5.1. Age of the Mesoproterozoic strata and its basement and cross-cutting units

A long-lasting debate exists about the age of the extensive, tabular siliciclastic units that overlie the Paleo- to Mesoproterozoic rocks of southwest Angola (Beetz, 1933; Carvalho, 1972; Carvalho and Alves, 1993; Correia, 1976; Mouta, 1954; Serv. Geol. Minas Angola, 1961; Vale, 1973a, 1973b). In this section, we address the depositional ages of the three studied siliciclastic units and discuss their mutual correlation and relation to the Mesoproterozoic Okapuka Formation of northwest Namibia.

5.1.1 Iona Group

The Iona Group has previously been correlated with the Okapuka Formation of northwest Namibia (Carvalho and Alves, 1993; Kröner and Correia, 1980; Labaredas et al., 2021). The Okapuka Formation unconformably overlies Paleoproterozoic migmatitic gneisses of the ENMC (Kröner et al., 2010, 2015). U-Pb dating of detrital zircons from the three Okapuka Formation samples provided a youngest MDA of 1324.1 ± 0.6 Ma, whereas a 1107 ± 4 Ma crosscutting leucodiorite provides a minimum depositional age (Kröner and Rojas-Agramonte, 2017).

The Iona Group quartz-arenite sample 418/101 gave an MDA of 1322.5 ± 13.4 Ma, which is identical to the MDA of the Okapuka Formation, supporting the idea that they are the same unit. The minimum depositional age of the Iona Group is further constrained by the crystallization age of 1222.2 ± 6.5 Ma for a crosscutting rhyolite porphyry (sample 418/50, Fig. 4F). The regional significance of a ~ 1.2 Ga magmatic event post-dating the sedimentation of the Iona Group is reinforced by the 1247.7 ± 6.7 Ma age of the alkali-feldspar porphyritic granite-gneiss (sample 440/94, Figs. 2 and 4E) and is consistent with previous reports of a regional magmatic event post-dating the deposition of the Iona Group (Carvalho and Alves, 1993; Serv. Geol. Minas Angola, 1961).

The Iona Group basement is newly constrained at 1516.9 ± 5. 3 Ma and 1517.1 ± 7.0 Ma (alkali-feldspar granite samples 418/48 and 418/100, Fig. 4C and 4D). Therefore, instead of being part of the Paleoproterozoic Regional Granite (e.g., Carvalho et al, 1984, 2000; Carvalho and Alves, 1993) our findings reveal that they belong to two distinct episodes of felsic Mesoproterozoic magmatism at ~ 1.52 and ~ 1.25–1.22 Ga in the Iona region. The Iona Group was deposited between these two episodes.

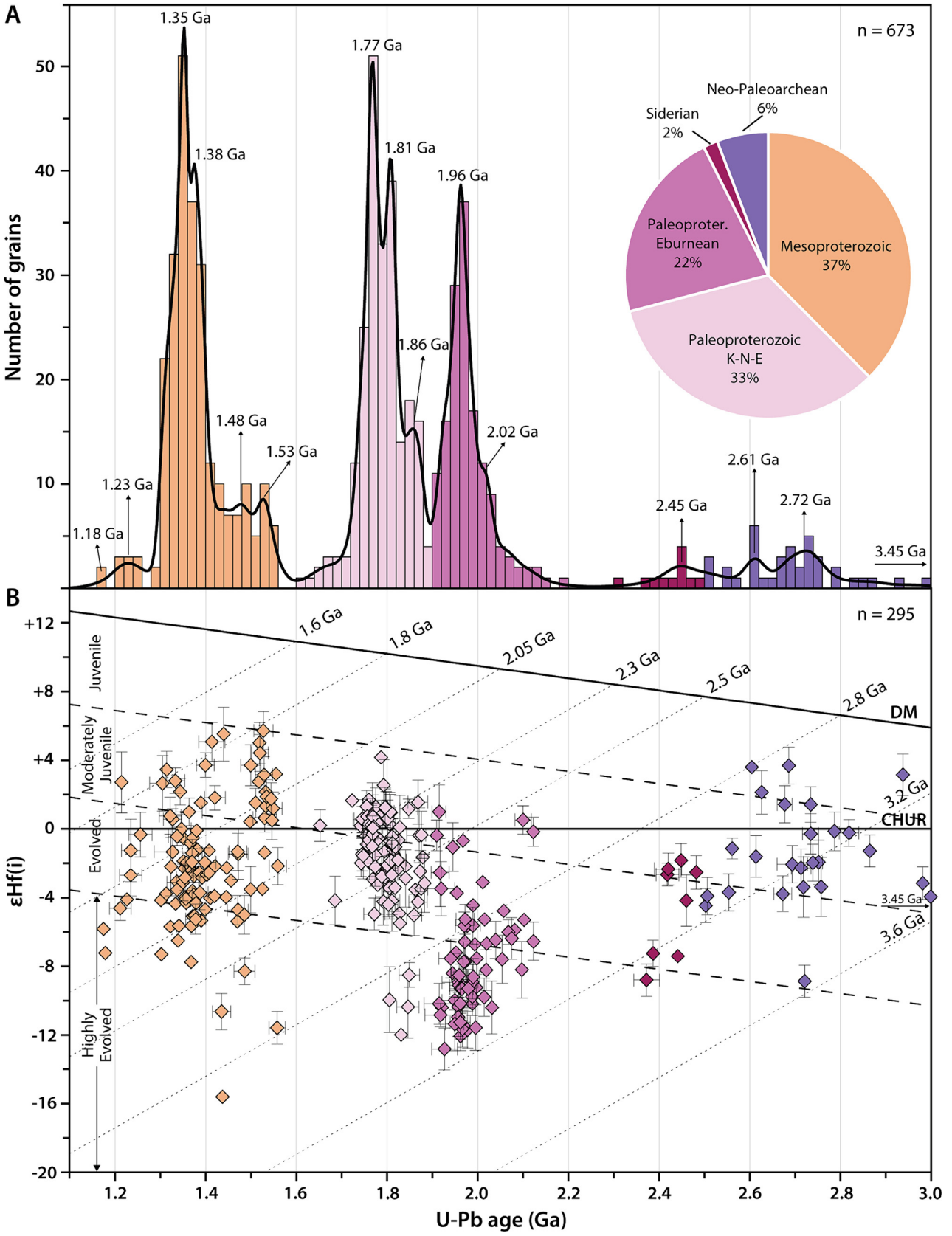

Fig. 7. (A) Adaptive kernel density estimation (KDE) plot and histogram displaying the distribution of the combined 673 concordant detrital zircon U-Pb ages obtained for the studied Mesoproterozoic strata. (B) U-Pb age versus $\varepsilon Hf_{(i)}$ plot for 295 detrital zircons (discordance = +5 to −2%) from the studied Mesoproterozoic strata. Detrital zircon groups are based on the main age clusters identified in this study. See text for further details.

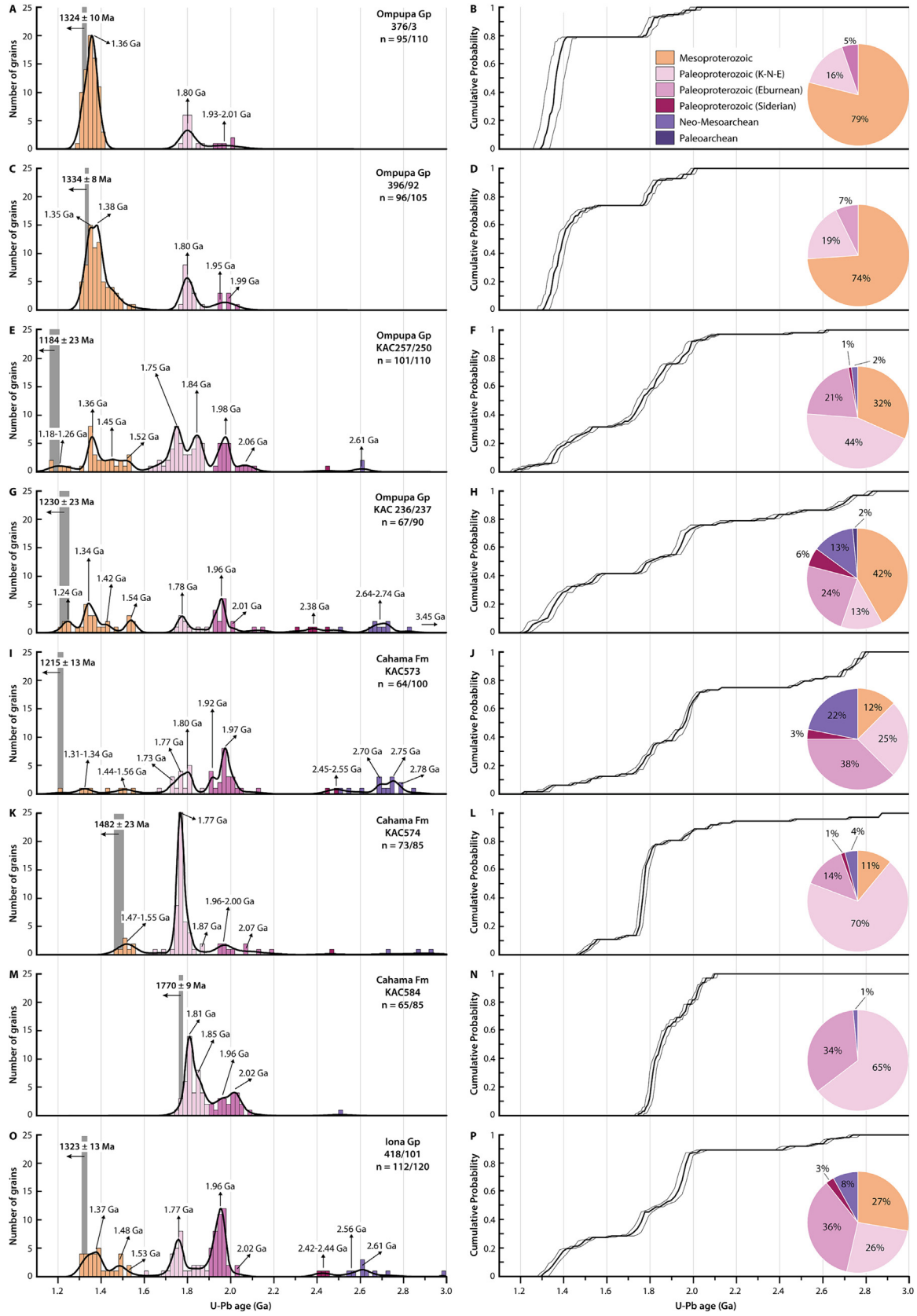

Fig. 8. Adaptative KDE and cumulative distribution function (CDF) plots showing the U-Pb age distribution of the concordant detrital zircons of the studied samples from the Ompupa Group (A to H), Cahama Formation (I to N) and Iona Group (O and P). Gray bars on the KDE diagrams represent the maximum depositional age (MDA) with associated ± 2σ uncertainty. Thin lines on the CDF diagrams correspond to the associated ± 2σ uncertainty.

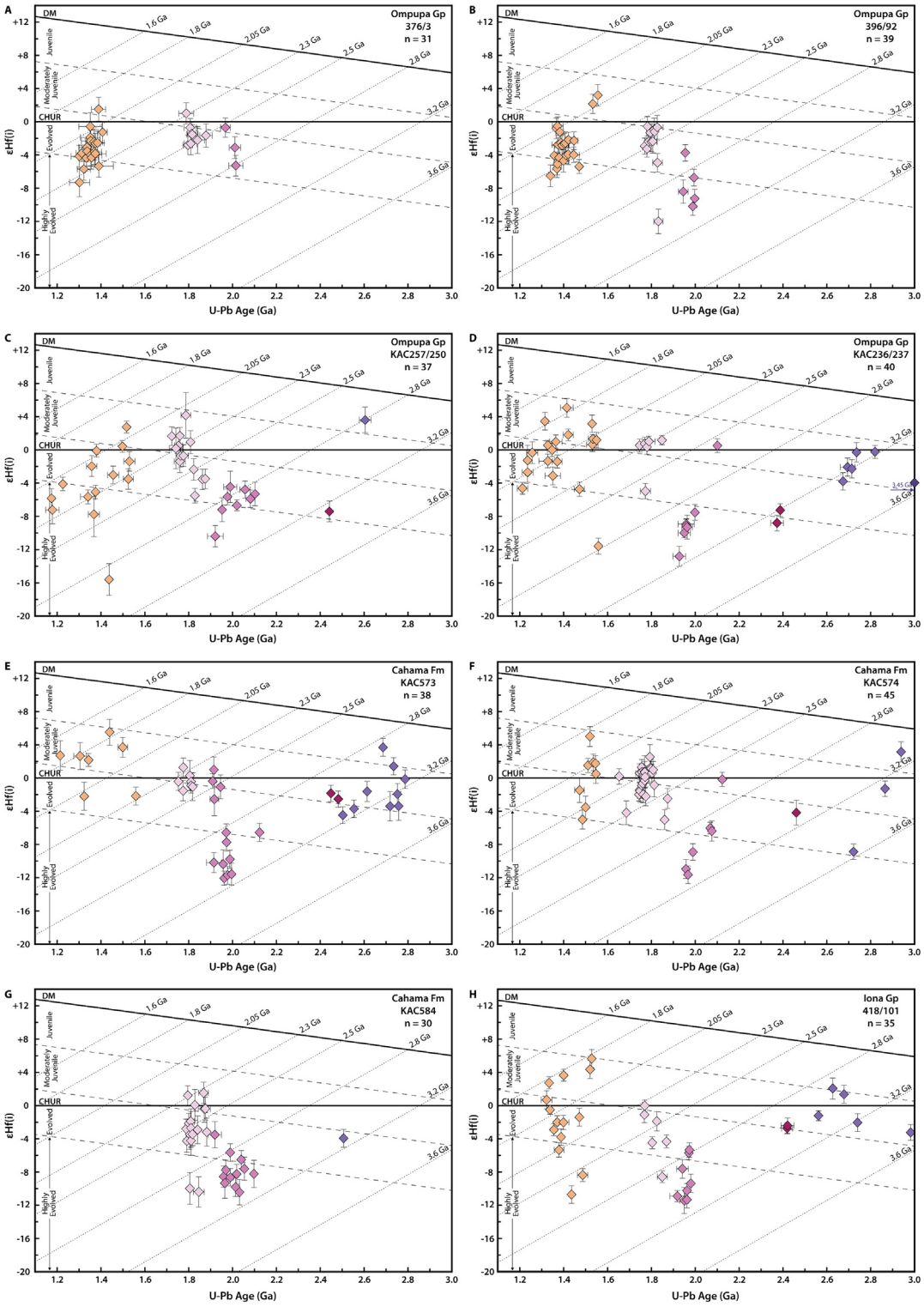

Fig. 9. U-Pb age versus $\varepsilon Hf_{(i)}$ diagram for representative detrital zircons (discordance = +5 to −2%) of the studied samples from the Ompupa Group (A to D), Cahama Formation (E to G) and Iona Group (H).

5.1.2 Ompupa group

The Ompupa Group rocks overlie ~ 1390 Ma Mesoproterozoic KC magmatic rocks (Bybee et al., 2019; Lehmann et al., 2020) and are cross-cut by 1119 ± 27 Ma (Rb-Sr whole-rock isochron age, Carvalho et al., 1987) or 1127 ± 8 Ma (U-Pb baddeleyite, Salminen et al., 2018) mafic dikes and sills (Fig. 2).

The four samples of the Ompupa Group gave two distinct MDA groupings according to their spatial position.

The first group, from the northernwestern part of the Ompupa Plateau, has an MDA of 1333.8 ± 8.3 Ma (sample 396/92) and 1324.1 ± 9.8 Ma (sample 376/3) and overlies 1811 ± 9 (sample 396/91) to 1796 ± 7 Ma (sample 976/59) basement granitoids.

The depositional age of these two samples is therefore bracketed between ~ 1.33 and 1.12 Ga, suggesting possible contemporaneity with the sedimentation of the Iona Group/Okapuka Formation. The second group, from the central and southeastern parts of the Ompupa Plateau, exhibits significantly younger MDAs of 1184.2 ± 22.6 Ma (sample KAC257/250) and 1229.9 ± 23.2 Ma (sample KAC236/237), respectively. These rocks are therefore younger than the Iona Group/Okapuka Formation, as well as younger than the regional felsic magmatism at ~ 1.25–1.22 Ga in the Iona region.

The absence of ~ 1.23–1.18 Ga detrital zircons in the northwestern samples (376/3 and 396/92) can be explained by: (i) their deposition prior to ~ 1.23 Ga, contemporaneous with the deposition of the Iona Group/Okapuka Formation, as suggested by the similarity of their MDAs; or (ii) the entire Ompupa Group was deposited between 1.18 Ga and 1.13 Ga, but the ~ 1.23–1.18 Ga zircons did not reach the depositional area of the northwest plateau due to unfavorable transport routes or because they were not present in the nearby source rocks. We favor the second hypothesis because of the textural and mineralogical immaturity of these sedimentary rocks (i.e., microconglomeratic lithic arkoses), which suggests a proximal source.

5.1.3 Cahama formation

The MDAs and detrital zircon age patterns of the three Cahama Formation samples are variable (Fig. 8). Sample KAC573 provided the youngest MDA of 1214.7 ± 13.3 Ma. Significantly older MDAs of 1482.2 ± 23.0 Ma and 1769.6 ± 9.4 Ma were obtained for samples KAC574 and KAC584, respectively. These older MDAs might reflect deposition prior (sample KAC584) or during (sample KAC574) the earliest stages of KC magmatism. Since our three samples have markedly different MDAs, the questions arises whether these three samples are from the same coherent stratigraphic unit, or the Cahama Formation is made-up of stratigraphic units of different age. Torquato and Salgueiro (1977) suggested that (at least part) of the Cahama Formation predates the intrusion of the Red Granite Suite. However, the lack of contact metamorphism in sedimentary rocks adjacent to the Red Granite Suite and the presence of clasts of Red Granite Suite in Cahama Formation siliciclastics rather supports that the Cahama Formation post-dates KC magmatism (Escuder-Viruete and Gumiel, 2021). Consequently, we interpret the Cahama Formation as a coherent stratigraphic unit, younger than the KC and deposited after 1.21 Ga. The differences in MDAs can be explained by source rocks containing different ages and the paucity in *syn*-KC or younger zircons reaching the sedimentary basin (11–12 % of Mesoproterozoic zircons in samples KAC573 and KAC574), compared to the Iona and Ompupa Groups samples (27–79 % of Mesoproterozoic zircons).

5.2. Detrital zircon provenance of the Mesoproterozoic strata

The studied Mesoproterozoic siliciclastic rocks of the AS were derived from nearby sources, with limited to no contributions from external sources as demonstrated by: (1) the excellent match between the age distribution of our combined U-Pb detrital zircon age spectra and the compilation of U-Pb crystallization ages of the southwest AS (Fig. 10); (2) the similarity between the Lu-Hf isotopic detrital zircon compositions with those published for the southwest AS (Fig. 11); (3) the detrital zircon age distribution from modern sand in northern Namibia (Gärtner et al., 2022) that reveals the same age distribution as our detrital and igneous zircon age compilation.

KDE, CDF, and MDS plots are commonly employed in detrital geochronology to assess provenance variability among detrital zircon samples and to constrain their sources (Andersen et al., 2018; Saylor et al., 2017; Spencer and Kirkland, 2016; Vermeesch, 2012, 2013; Vermeesch and Garzanti, 2015; Wissink et al., 2018). Whereas KDE and CDF are utilized for visualizing zircon age distributions, MDS transforms pairwise dissimilarities between these distributions into distances in a multi-dimensional space, resembling a 2D or 3D map. In this "map", samples are depicted as points, with the separation between two points indicating the degree of dissimilarity between their zircon age distributions. In simple terms, samples with similar zircon age distributions are positioned closer together, whereas those with distinct distributions are situated farther apart.

We employ KDE, CDF, and MDS plots to evaluate the provenance variability of the studied Mesoproterozoic detrital samples alongside potential Mesoproterozoic to Archean sources from the SW Angolan Shield (Fig. 12). The zircon age data considered for potential source areas of the SW Angola Shield include published U-Pb data from the crystalline basement used for Fig. 10B, as well as (limited) detrital zircon U-Pb age data available for Paleoproterozoic supracrustal rocks of the Chela Group and the Orue, Epembe, and Eyao units of the ENMC (Brandt et al., 2021; Kröner et al., 2015; Seth et al., 2003, 2005). The KDE and CDF diagrams reveal that the studied samples can be broadly categorized into two main types based on their age distribution patterns (Fig. 12A and B).

5.2.1. Type-1: Dominant prevalent proximal source age mode

Samples 376/3, 396/92, KAC574, and KAC584 exhibit prominent age modes, implying that their detrital zircons are likely derived from a relatively limited area and from a prevalent proximal source. These samples can be further subdivided into two subtypes based on the age of their main age peak: Mesoproterozoic (subtype 1A: samples 376/3 and 396/92), and K-N-E (subtype 1B: samples KAC574 and KAC584).

5.2.1.1. Subtype-1A: Dominant Kunene Complex age mode. Northwest Ompupa Plateau samples (376/3 and 396/92) are dominated by Mesoproterozoic zircons with a main peak at ~ 1.38–1.36 Ga, accompanied by two smaller K-N-E and Eburnean peaks. Their age distribution is statistically indistinguishable at 95 % confidence level (p-value = 0.089; Supplementary Data, Table S6A), indicating that they originate from the same sources.

Nearly half of the total number of dated Mesoproterozoic zircons is sourced from the KC (~1.50–1.36 Ga; Figs. 11, 12A and C). The other half corresponds to zircon ages younger than the KC, and there are two zircon grains at ~ 1.54 Ga. Deconvolution of the Mesoproterozoic ages reveals the existence of discrete Mesoproterozoic age peaks at ~ 1.54, 1.46, 1.41, 1.38, and 1.33 Ga (Supplementary Data, Figure S5). The two detrital zircons dated at ~ 1.54 Ga were likely derived from the similar-aged pre-KC granitoids found in the Iona region and northwestern Namibia, whereas the three middle peaks can be directly related to the KC (Figs. 11 and 12A). Interestingly, the youngest age peak at ~ 1.33 Ga is only represented in the Orue Unit upper-amphibolite facies metamorphism of the ENMC (~1.34–1.32 Ga), which is a minor contributor to the currently available zircon budget of the AS. The Orue Unit metamorphism age range is also present in other detrital zircon samples of this study (samples 418/101, KAC257/250, KAC236/237, and KAC573) and in northwest Namibia (Okapuka Formation), indicating that ~ 1.34–1.32 Ga zircon-bearing magmatic rocks could be more common than is currently known, either having undergone erosion, or yet to be identified in poorly mapped regions, and/or being concealed under the extensive Kalahari cover.

The small K-N-E detrital zircon age peaks can be explained by a source in the local Paleoproterozoic ENMC granitoids and orthogneisses, which have identical age and zircon Hf isotopic compositions (Figs. 11 and 12A). However, erosion of these rocks does not explain the Eburnean peak as, to date, no Eburnean magmatic rocks have been identified in the ENMC (Kröner et al., 2010, 2015;

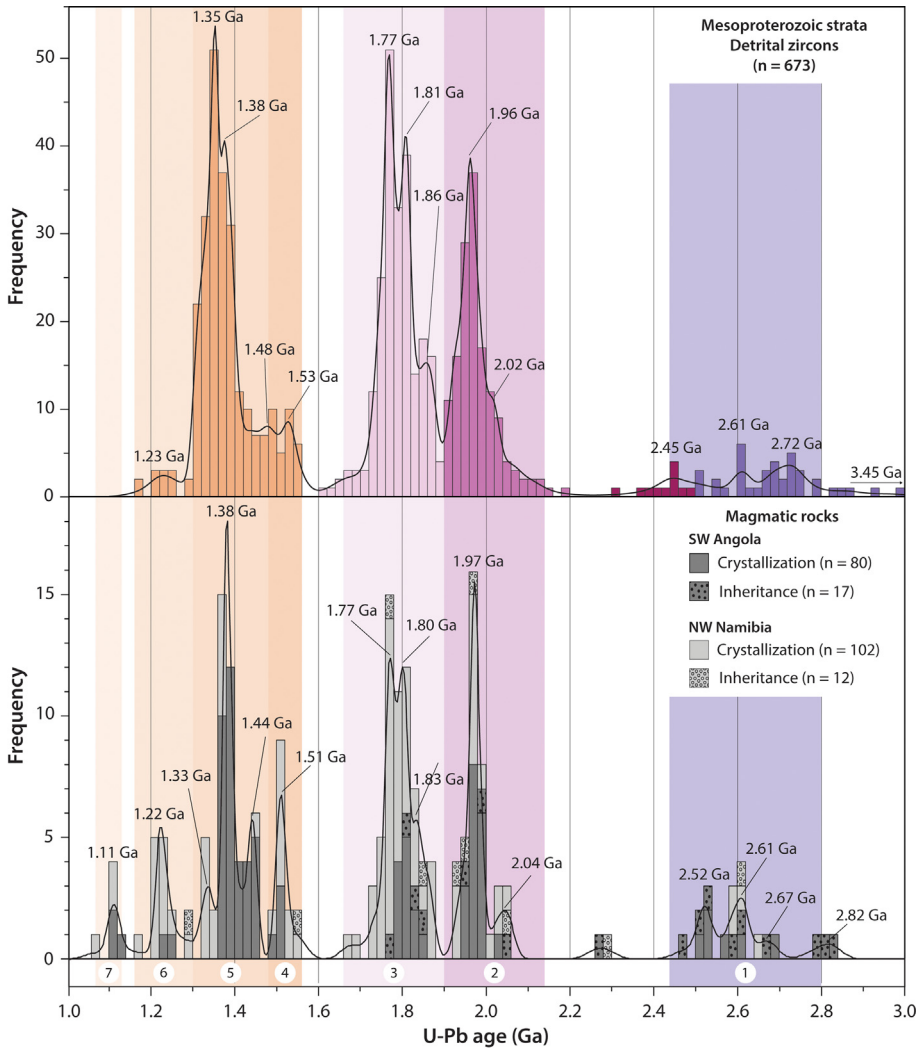

Fig. 10. Comparison between the adaptive KDE plots and histograms of the combined 673 concordant detrital zircon U-Pb ages from the studied Mesoproterozoic strata (A) and the available crystallization and inherited ages for magmatic and *ortho*-derived rocks of the SW Angolan Shield (B). Main periods of magmatism in the SW Angolan Shield: Archean to Early Siderian (1); Paleoproterozoic Eburnean (2) and Kamanjab–Namibe–Epupa (3); Mesoproterozoic pre-Kunene Complex (4), Kunene Complex (5), post-Kunene Complex (6), and Umkondo-related mafic dikes and sills (7). References for the KDE in Fig. 10B are the same as for Fig. 1.

Rodrigues et al., 2021a), requiring an additional, albeit minor, source of Eburnean zircons in these samples. Based on our current knowledge, potential sources of Eburnean zircon include (Figs. 1 and 12A): (i) Eburnean granitoid/orthogneisses and Chela Group supracrustal rock of the CEZ; (ii) Eburnean granitoid (and supracrustal rock?) of the CZ; (3) the Sesfontein, Kamanjab, Grootfontein, Tsumkwe and Quangwadum inliers; (4) the nearby ENMC Paleoproterozoic supracrustal rocks and, potentially, the Namibe Group; (v) rare xenocrysts in the KC (Milani et al., 2022). Given the proximal character of these samples, Eburnean zircons were likely sourced from the nearby ENMC supracrustal rocks, the Namibe Group, and/or the xenocrysts within the KC.

5.2.1.2. Subtype-1B: Dominant K-N-E age mode. Cahama Formation samples KAC574 and KAC584 exhibit a prominent K-N-E age mode. However, the KAC574 main peak age is 1.77 Ga, whereas it is 1.81 Ga for KAC584 (Fig. 12A). This difference suggests distinct sources, which is confirmed by the MDS plot, as the two samples plot at a considerable distance (Fig. 12C), and the K-S test, which underscores significant dissimilarity (p-value = 0; Supplementary Data, Table S6A). The sources of sample KAC 574 zircons are the ENMC Paleoproterozoic supracrustal rocks and the Paleo- to Mesoproterozoic ENMC granitoid/orthogneiss, as shown by the intermediate position of the sample between these two source poles in the MDS space (Fig. 12C). Although the Kamanjab Inlier appears to be the most probable source for sample KAC584 based on their statistical similarity (p-value = 0.071; Supplementary Data, Table S6A) and position in the MDS space (Fig. 12C), its distant location, ~300 km away, is inconsistent with the sample's proximal characteristics. Hence, the presence of an unidentified nearby source sharing a similar zircon age distribution with the Kamanjab Inlier is suggested.

5.2.2. Type-2: Diverse age distribution

Samples 418/101 (Iona Group), KAC257/250 and KAC236/237 (central and southern Ompupa Group) and KAC573 (Cahama Formation) exhibit detrital zircon age spectra ranging from Archean to Mesoproterozoic that are significantly more diverse and heterogeneous than those of Type-1 samples (Fig. 12A and B), suggesting enhanced basin connectivity and a larger catchment area. Despite this heterogeneity, Type-2 samples essentially share the same age groups, indicating that they likely share common sources, with the variation in peak age proportions resulting from random sampling of the same parent populations. This is further supported by their distinct positions within the MDS space relative to the defined potential sources (Fig. 12C).

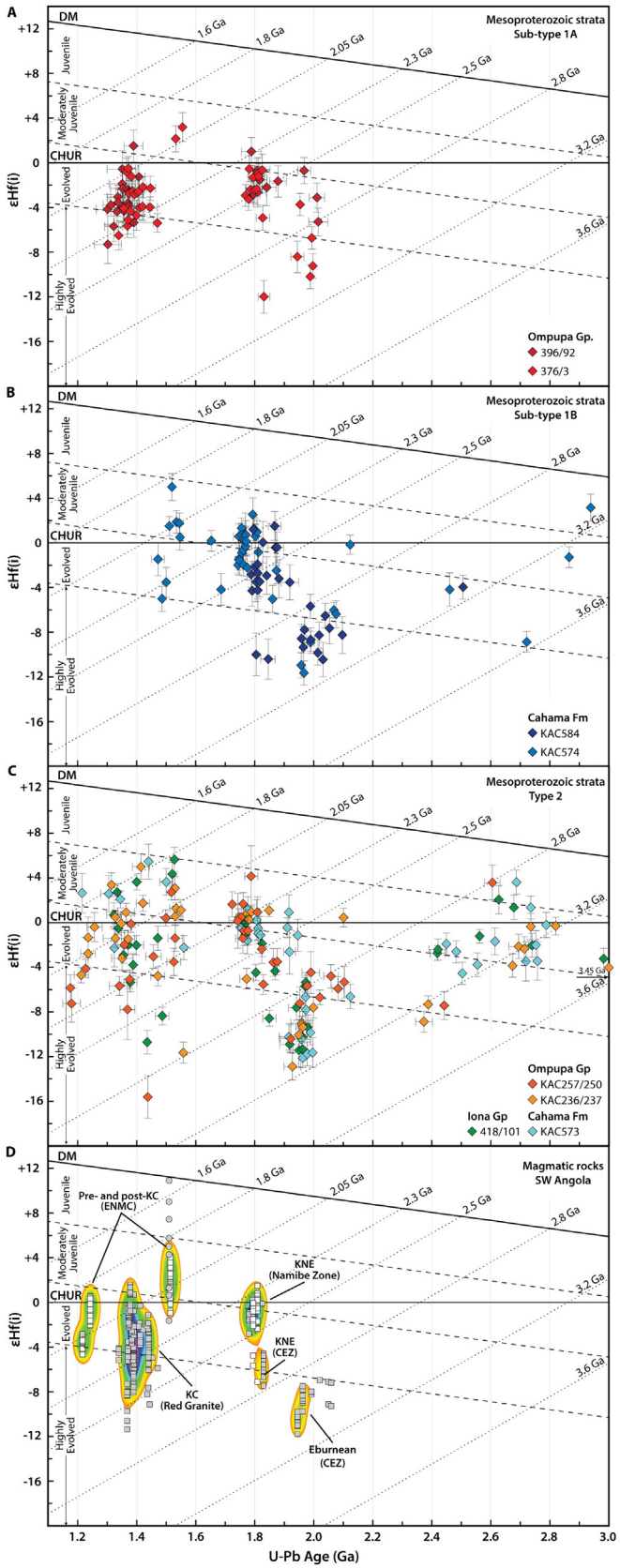

Fig. 11. U-Pb age versus $\varepsilon Hf_{(i)}$ diagram for the detrital zircons of the Mesoproterozoic strata (A, B and C) and the potential sources in the Angolan Shield (D). Data in Fig. 11D are from this study (white squares), Jung et al., (2012; gray circles) and Milani et al., (2022; gray squares). Sedimentary samples in Fig. 11A, B and C are grouped according to their U-Pb detrital age distribution type (see details in section 5.2). Heat maps in Fig. 11D correspond to the 90% data contour.

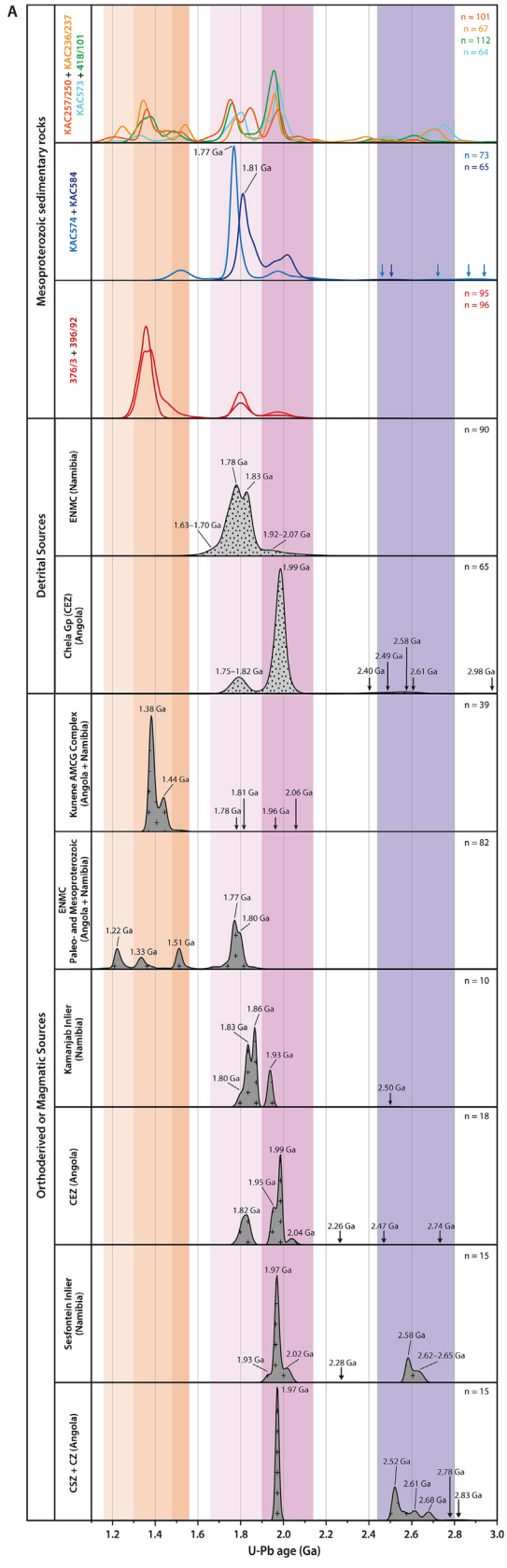

Fig. 12. KDE (A), CDF (B) and MDS (C) diagrams comparing the U-Pb age distribution of the studied Mesoproterozoic strata and potential Mesoproterozoic to Archean sources of zircon from the SW Angolan Shield (references for literature data are the same as for Fig. 1). The studied sedimentary samples are grouped according to their U-Pb detrital age distribution type (see details in section 5.2). The potential detrital and magmatic/*ortho*-derived sources of zircon from the SW Angolan Shield depicted in the KDE plots of Fig. 12A are represented in the MDS diagram of Fig. 12C as light-grey dotted circles and as dark-grey circles with crosses, respectively.

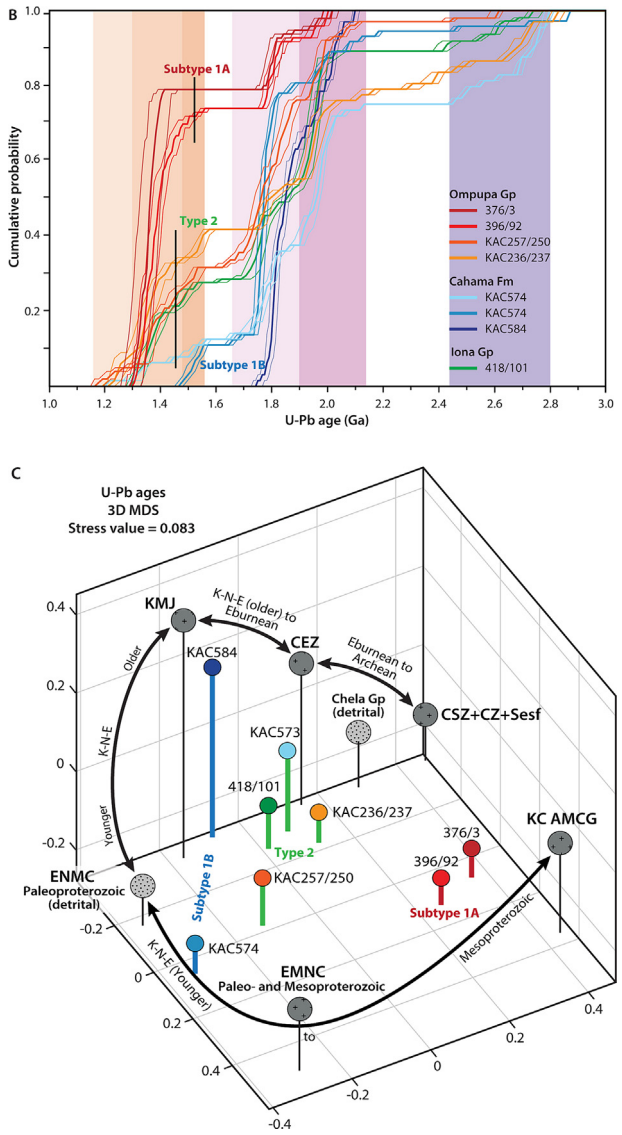

Fig. 12 (*continued*)

Samples 418/01, KAC236/237. KAC573 and sample KAC257/250 differ in their Paleoproterozoic zircon distribution, with distinct Eburnean vs K-N-E ratios. Samples 418/101, KAC236/237, and KAC573 display a predominance of Eburnean over K-N-E zircon, alongside significant proportions of early Siderian to Archean zircon (Fig. 12A and B). Markedly distinct Hf isotopic compositions suggest different source regions for K-N-E and Eburnean zircons (Fig. 11C and 13). Provenance of K-N-E zircons is primarily from Paleoproterozoic supracrustal rocks (Fig. 12A) and surrounding ENMC granitoids/orthogneisses (Fig. 11D), with a minor contribution from the CEZ—as suggested by the presence of limited K-N-E zircon with very negative $\varepsilon Hf_{(i)}$, which overlaps with the zircon Hf composition of CEZ K-N-E granitoids (Fig. 11C and D). A shared source of Eburnean and Siderian-Archean zircons is supported by U-Pb and $\varepsilon Hf_{(i)}$ data as they follow the same crustal evolution trend (Fig. 11C, D and 13A). Eburnean and Archean rocks in the southwest AS are currently exposed together only in the CSZ and CZ (Angola) and in the Sesfontein Inlier (Namibia) (Figs. 1, 12A). Archean xenocrysts, inherited cores, and/or Nd- or Hf-TDM_2 ages in Eburnean rocks (Kröner, 2005; Luft et al., 2011; Milani et al., 2022; Pereira et al., 2011; Sanz, 2005; Seth, 1999; Singletary et al., 2003) reveal that the Angolan CEZ and the northern Namibia/NW Botswana Paleoproterozoic inliers (Kamanjab–Grootfontein–Tsumkwe–Quangwadum) have concealed Archean rocks. However, the absence of Hf zircon data for these zones (except for the CEZ) hinders the identification of the precise source(s) of Eburnean to Archean zircon in our Mesoproterozoic rocks.

Unlike the previous samples, sample KAC257/250 exhibits a predominance of K-N-E over Eburnean zircon (and minimal quantities of Siderian and Archean zircon), consistent with a prevalent ENMC source. This is supported by the sample position within the MDS space (Fig. 12C), where it plots closer to the ENMC detrital and granitoid/orthogneiss poles compared to samples 418/101, KAC236/237, and KAC573, which deviate towards the Eburnean to Archean poles (CEZ, Chela Group, and CSZ + CZ + Sesfontein).

Despite varying amounts of Mesoproterozoic zircon, Type-2 samples share a consistent age range (1.56–1.31 Ga) and Hf compositions (Figs. 8, 11C and 12A). This suggests that their Mesoproterozoic zircons originate from the same sources, such as pre-KC granitoid (~1.55–1.50 Ga), KC anorthosite and Red Granite Suite (~1.50–1.36 Ga), and potential Orue-aged magmatism (~1.34–1.32 Ga). The Ompupa and Cahama samples (KAC236/237, KAC257/250 and KAC573) show an additional contribution from ENMC ~ 1.29–1.18 Ga granitoid and alkaline-carbonatite (Kröner and Rojas-Agramonte, 2017; Litmann et al. 2000; Simon et al., 2017; Tshiningayamwe et al., 2022; this study), which is missing in the Iona Sample (418/01) because the latter was deposited before these younger plutons formed (Fig. 8; see section 5.1).

5.3. Spatial and temporal evaluation of the u-pb and Lu-Hf data: Insights into the crustal evolution of the southwest Angolan Shield

The combined U-Pb ages and Lu-Hf isotopic data from detrital zircons in Mesoproterozoic sedimentary rocks (this study), along with U-Pb ages, Lu-Hf, and/or Sm-Nd isotopic data from Archean to Mesoproterozoic magmatic rocks (Baxe, 2007; Brandt et al., 2021; Bravo Silva et al., 2021; Bybee et al., 2019; Campeny et al., 2023; Drüppel et al., 2007; Ernst et al., 2013; Escuder-Viruete and Gumiel, 2021; Franz et al., 1999; Galán, 2021; Goscombe et al., 2005; Gutiérrez-Medina et al., 2021; Hoal et al., 2000; Jelsma et al., 2018; Kröner et al., 2015, 2010, 2004; Kröner and Rojas-Agramonte, 2017; Langa, 2019; Lehmann et al., 2020; Littmann et al., 2000; Luft et al., 2011; Maier et al., 2013; Máximo et al., 2021a; Mayer et al., 2004; McCourt et al., 2013; Merino-Martínez and Goicoechea, 2021; Milani et al., 2022; Pereira et al., 2011; Salminen et al., 2018; Sanz, 2005; Seth, 1999; Seth et al., 2005, 2003; Simon et al., 2017; Singletary et al., 2003; Tshiningayamwe et al., 2022; this study) (Figs. 1, 13 and 14), offer a new opportunity to investigate the Archean to Mesoproterozoic crustal evolution of the southwest Angolan Shield. When interpreted in light of the current understanding of crustal evolution trends from modern and ancient orogens derived from Lu-Hf and Sm-Nd data, our dataset allows us to propose an Archean to Mesoproterozoic geodynamic evolution for the southwest Angolan Shield. Indeed, a large body of recent work shows that different geodynamic settings have different propensities for either crustal reworking or addition of mantle-derived juvenile magmas. Extension-dominated settings, associated with continental breakup or accretionary margin orogens, display progressively more radiogenic Nd–Hf isotopic values over time due to the increasing influence of juvenile mantle melts caused by extension-driven lithospheric thinning; in contrast, contraction-dominated settings, associated with continent–continent collision or compressional phases of accretionary margin orogens, exhibit progressively more unradiogenic isotopic compositions over time as crustal thickening promotes more extensive crustal melting and/or assimilation of juvenile mantle melts (Chapman et al., 2017; Collins et al., 2011; Kemp et al., 2009; Kohanpour et al.,

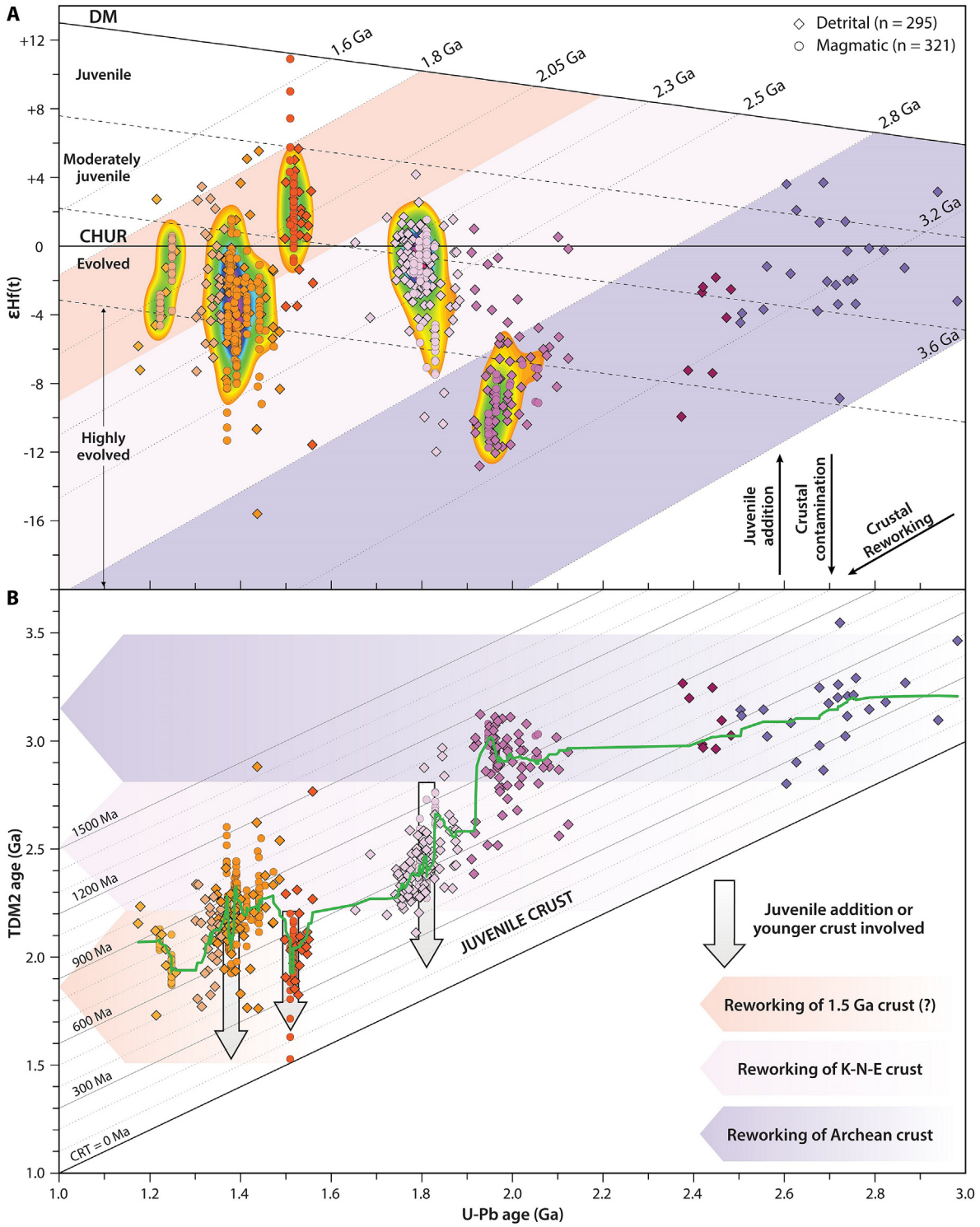

Fig. 13. U-Pb age versus $\varepsilon Hf_{(i)}$ (A) and two-stage depleted mantle model ages (B) for detrital (diamonds) and igneous (circles) zircons from the SW Angolan Shield (references for literature data are the same as in Fig. 11). Heat maps in Fig. 14A correspond to the 90 % data contour. Green line in Fig. 14B corresponds to the moving-median (period = 20) considering the whole dataset (detrital + igneous zircons). (For interpretation of the references to colour in this figure legend, the reader is referred to the web version of this article.)

2019; Roberts and Spencer, 2015; Spencer et al., 2013, 2019; Sundell and Macdonald, 2022).

5.3.1. Archean to early Siderian crustal reworking and minor juvenile addition

Despite spanning a wide age range and comprising only a minor component in the Mesoproterozoic strata (Fig. 10), Archean to early Siderian detrital zircons (~3.45 to 2.30 Ga) provide valuable insights into the evolution of the southwest AS. Peaks in detrital and igneous zircon U-Pb ages occur at 2.82, 2.72, 2.61, 2.52, and 2.45 Ga (Fig. 10), revealing distinct (some yet to be identified) magmatic events in the southwest AS. Most zircons (88 %) exhibit moderately juvenile to evolved $\varepsilon Hf_{(i)}$, consistent with the involvement of older crustal material in their formation. Interestingly, their

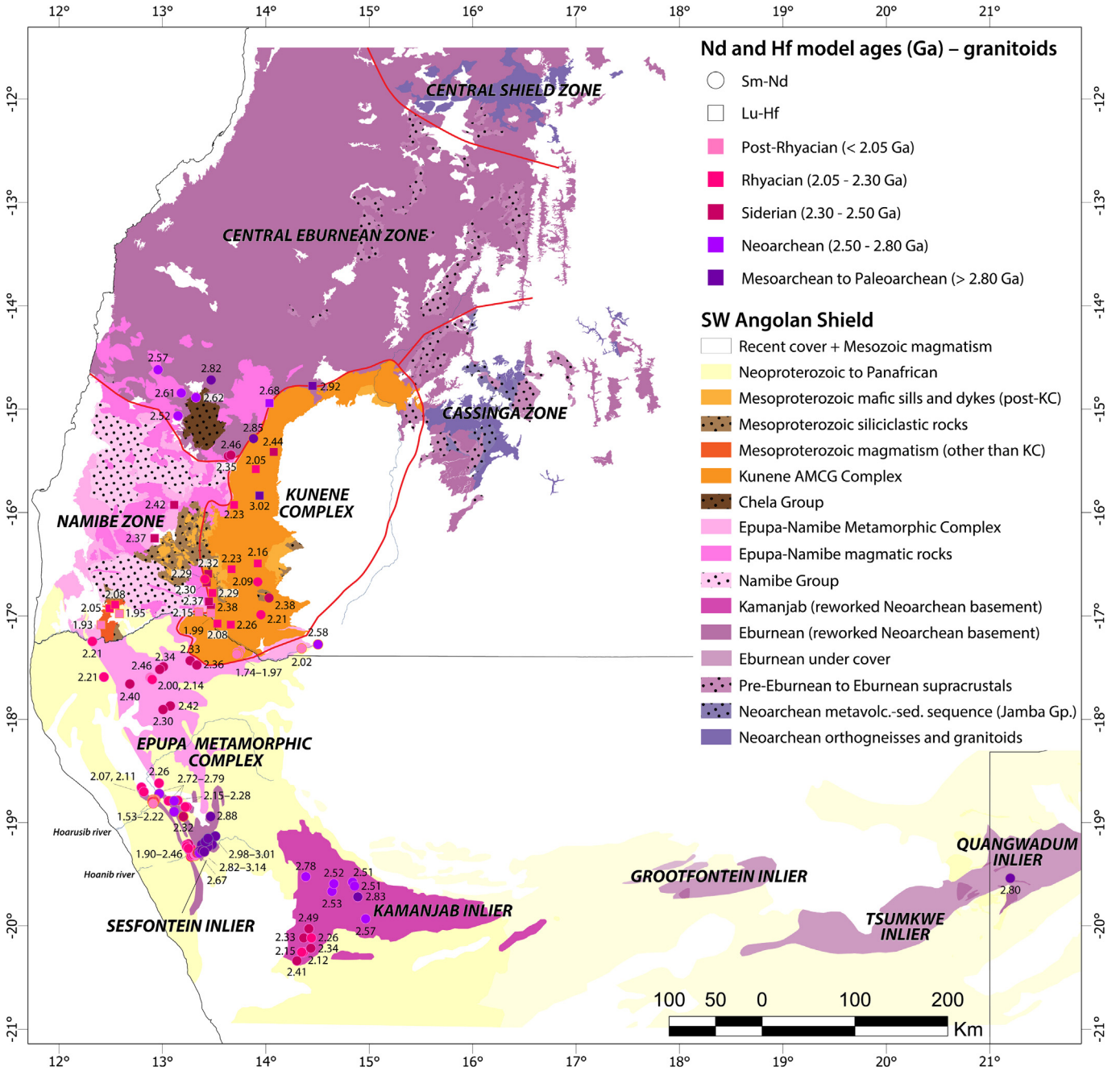

Fig. 14. Spatial distribution of two-stage depleted-mantle Nd- and Hf-model ages (TDM_2) for intermediate to felsic rocks of the Angolan Shield. The border colour of the symbols corresponds to the crystallization age of the samples (Archean, Eburnean, K-N-E, and Mesoproterozoic). References for the reported published Sm-Nd and Lu-Hf TDM_2 ages are Seth (1999), Singletary et al. (2003), Baxe (2007), Kröner (2005), Drüppel et al. (2007), Janoušek et al. (2010), Kröner et al. (2010), Luft et al. (2011), Pereira et al. (2011), Jung et al. (2012), Kleinhanns et al. (2013), Milani et al. (2022), Campeny et al. (2023), this study.

$\varepsilon Hf_{(i)}$ values generally decrease with younger U-Pb ages, hinting at successive reworking of crust extracted from mantle sources in the Meso- to Paleoarchean (Fig. 13). This reworking is further supported by the Mesoarchean Nd-TDM_2 ages (3.01–2.98 Ga) of the ~ 2.65 to 2.58 Ga orthogneisses in the Sesfontein Inlier (Seth, 1999) and the presence of inherited Mesoarchean zircons (2.82 Ga) in Eburnean granitoid intrusive into Neoarchean granitoid of the CSZ (Jelsma et al., 2018) (Figs. 1 and 14). Despite the predominance of crustal reworking, minor juvenile magmatism also occurred during the Meso- to Neoarchean period, as evidenced by five Neoarchean (2.73–2.60 Ga) and one Mesoarchean (2.94 Ga) detrital zircons displaying suprachondritic $\varepsilon Hf_{(i)}$. The origin of this juvenile magmatism in the southwest AS is yet to be identified.

5.3.2. Eburnean crustal reworking and K-N-E juvenile magmatism

The basement of the southwest AS is dominated by Paleoproterozoic granitoid formed between ~ 2.05 and 1.73 Ga (Figs. 1 and 10B; e.g., Carvalho et al., 2000; Hoal et al., 2000; Jelsma et al., 2018; Kleinhanns et al., 2013; Kröner et al., 2015, 2010, 2004; McCourt et al., 2013; Pereira et al., 2011; Seth, 1999; Singletary et al., 2003). Our compilation of zircon U-Pb magmatic ages (Fig. 10B), supported by the detrital zircon age distribution in the Mesoproterozoic strata (Fig. 11A), reveals two main Paleoproterozoic age clusters: (i) Eburnean magmatism (~2.05–1.93 G a) with a large peak at 1.97 Ga and a small peak at 2.04 Ga; and (ii) K-N-E magmatism (~1.87–1.73 Ga) with peaks at 1.86, 1.83, 1.80, and 1.77 Ga. However, two slight differences are observed

in the detrital zircon U-Pb ages compared to igneous zircon: (i) the K-N-E cluster extends to younger ages, down to ~ 1.62 Ga, likely due to the presence of ~ 1.63–1.70 Ga detrital zircon cores from ENMC supracrustal rocks (Seth et al., 2003, 2005) and zircon from rare ~ 1.68–1.67 Ga post-tectonic granitic dikes in the ENMC (Kröner et al., 2004, 2010); and (ii) the Eburnean cluster exhibits an older tail, with ages up to ~ 2.18 Ga from unidentified sources that could include presently undated Paleoproterozoic supracrustal sequences (e.g., Namibe, Chivanda, Vila Branca, N'Gola, Utente-Cela, Oendolongo, and Bale Groups; Merino-Martínez et al., 2021 and references therein).

The southwest Angolan Shield is currently interpreted as a long-lived Andean-type continental arc (~2000 ± 200 Ma) at the southwestern margin of the Congo Cracton (Jelsma et al., 2018; Kleinhanns et al., 2013; Kröner et al., 2015; McCourt et al., 2013; Seth, 1999). In this work, we recognize two contrasting and sequential Paleoproterozoic settings, distinguished by differences in the spatial distribution of U-Pb ages and the Nd-Hf isotopic signature of the Eburnean and K-N-E magmatism.

5.3.2.1. Eburnean (~2.05–1.93 Ga): Prevalent crustal reworking in the early Orosirian. Most Eburnean detrital zircons (84 %) show highly evolved Hf compositions (markedly negative $\varepsilon Hf_{(i)}$ values and Mesoarchean TDM_2 ages), matching those found in ~ 1.96 Ga CEZ Eburnean granitoid and a ~ 1.95 Ga Eburnean granitoid septum in the northern KC (Milani et al., 2021). Their Hf compositions further follow the same crustal evolution trend as early Siderian to Archean zircon preserved in the Mesoproterozoic strata (Figs. 13 and 14). This suggests that Eburnean zircon in the southwest AS formed by reworking of older crust, extracted from the depleted mantle in Mesoarchean times, with minimal addition of juvenile material (Figs. 13 and 14). Crustal reworking is further supported by the presence of ~ 2.83 to 2.50 Ga U-Pb zircon xenocrysts/cores and Meso- to Neoarchean Nd-TDM_2 ages in Eburnean granitoids across various locations: CSZ, CEZ, Hoarusib-Hoanib rivers area, Kamanjab and Quangwadum inliers (Janoušek et al., 2010; Jelsma et al., 2018; Kröner, 2005; Luft et al., 2011; Milani et al., 2022; Pereira et al., 2011; Sanz, 2005; Seth, 1999; Singletary et al., 2003).

The highly evolved Hf–Nd composition of Eburnean magmas is compatible with petrogenesis in a collisional orogenic setting, possibly related to amalgamation of independent Archean crustal blocks of the southwest AS (e.g., CZ, CSZ, Sesfontein inlier; Merino-Martínez et al., 2021; Rodrigues et al., 2021). Jelsma et al. (2018) proposed that peak metamorphism and deformation of the Archean crust occurred during the Eburnean orogeny at ~ 1.97 Ga based on a peak in igneous zircon ages, which also corresponds with the peak of Eburnean detrital zircons (Fig. 10). This hypothesis gains further support from recent U-Pb dating of migmatite from the CSZ and CEZ, also yielding ~ 1.97 Ga (Merino-Martínez et al., 2021; Rodrigues et al., 2021b). Therefore, the ~ 1.97 Ga peak likely represents the apex of collisional magmatism in the southwest AS.

5.3.2.2. Kamanjab–Namibe–Epupa (~1.87–1.73 Ga): A late Orosirian to early Statherian accretionary margin in the southwest Angolan Shield?. Our study shows that the ENMC is a younger (1.87–1.73 Ga; Fig. 1) and distinct isotopic domain within the southwest AS, characterized by significantly more radiogenic magmatism compared to the Eburnean and Archean crust (Figs. 13, 14, and Supplementary Data Figure S6). Notably, the predominantly slightly subchondritic to suprachondritic Hf and Nd isotopic compositions preserved in most K-N-E zircons and granitoids correspond to an average decrease of ~ 700 to 600 Myr in TDM_2 age relative to their Eburnean and Archean equivalents. Interestingly, the only Hf and Nd isotopic compositions approaching the more evolved composition of the Eburnean and Archean crust are restricted to K-N-E granitoids intrusive into the abutting CEZ and Kamanjab Inlier, located at the northern and southern margins of the ENMC. This suggests variable hybridization processes between juvenile K-N-E magmas and evolved crustal components of the CEZ and Kamanjab Inlier. Therefore, the more radiogenic character of the ENMC K-N-E granitoids compared to those of the CEZ and the Kamanjab Inlier could result from the melting of a distinct juvenile crust that now forms the unexposed basement of the ENMC.

Two hypotheses are proposed to explain the distinct isotopic signature of the ENMC crust. The first suggests that the ENMC corresponds to a younger allochthonous Paleoproterozoic terrane with a distinct and independent evolutionary history prior to K-N-E magmatism. This terrane accreted to the southwest AS's Eburnean-Archean crust (currently represented by the CEZ) during the late Orosirian period, undergoing subsequent reworking and rejuvenation until the early Statherian (~1.73 Ga). However, as noted by McCourt et al. (2013), considering the ENMC as an allochthonous terrane before K-N-E magmatism implies an allochthonous origin for the Eburnean-Archean inliers located to the south of the ENMC (Sesfontein, Kamanjab, Grootfontein, Tsumkwe, and Quangwadum). The second hypothesis suggests that the ENMC is related to an extensional accretionary orogen developed synchronously with K-N-E magmatism along the southern margin of the southwest AS's Eburnean-Archean crust, analogous to the Paleozoic Australian Lachlan Orogen (e.g. Kemp et al., 2009). K-N-E detrital zircon (~1.87–1.73 Ga) shows a correlation between younger ages and increasing radiogenic Hf composition (Fig. 13), which seems to support the second hypothesis. A back-arc scenario provides a plausible explanation for this trend because we expect a progressive addition of juvenile material alongside reduced crustal influence as the subduction zone migrates away from the Eburnean–Archean continental margin.

5.3.3. Mesoproterozoic

Magmatism in the southwest AS resumed in the early Calymmian (~1550 Ma) following a ~ 200 Myr period of magmatic quiescence and persisted in variable intensity and nature until the late Stenian (~1110 Ma) (Fig. 10B).

5.3.3.1. Early Calymmian juvenile magmatism (~1.55–1.50 Ga) to mixed crustal to juvenile magmatic signatures during emplacement of the Kunene Complex (~1.50–1.36 Ga). The earliest Mesoproterozoic magmatism at ~ 1.55 to 1.50 Ga (Fig. 10B) is marked by minor A-type granitoid in the ENMC (Kröner et al., 2015; Kröner and Rojas-Agramonte, 2017; this study) and the Hoarusib-Hoanib rivers area (Jung et al., 2012; Kröner et al., 2004; Luft et al., 2011; Seth, 1999), mafic dikes crosscutting the Chela Group (Ernst et al., 2013) and the ENMC (Seth et al., 2003), and an evolved pegmatoidal pod hosted in central KC anorthosite (Bybee et al., 2019). The extensive geographic distribution of early Mesoproterozoic magmatism across the EMNC, CEZ and KC (Fig. 1), and its synchronicity with 1.53–1.51 Ga UHT-HP metamorphism (~1000 °C and 9.5 kbar) in the ENMC Epembe Unit (Brandt et al., 2007, 2021; Seth et al., 2003) suggest the existence of a regional thermal event in the southwest AS, possibly starting as early as ~ 1.56 Ga, as indicated by the detrital zircon record (Fig. 10A).

Early Mesoproterozoic magmatism is juvenile, as demonstrated by positive $\varepsilon Hf_{(i)}$ values of most detrital zircons (~1.56–1.50 Ga) preserved in the Mesoproterozoic strata (this study), as well as the igneous zircons from ~ 1.52–1.50 Ga granitoids of the Iona region (this study) and the Hoarusib-Hoanib rivers area (Jung et al., 2012) (Figs. 11 and 13). Despite the dominance of juvenile input, there are a few detrital zircons with Hf compositions mirroring the K-N-E crustal evolution trend (Fig. 13). This is consistent with the occurrence of ~ 1.79 Ga xenocrysts in a ~ 1.53 Ga granitoid dated along the Kunene River (Kröner et al., 2015), indicating

contamination by or remelting of ENMC crust during emplacement of the early Mesoproterozoic juvenile magmatism (Fig. 13).

After the dominant period of juvenile addition between ~ 1.56 and 1.50 Ga, the detrital and igneous zircons associated with the KC (~1.50–1.36 Ga) exhibit a significant shift toward more evolved Hf isotopic compositions until ~ 1.45 Ga (Fig. 13). These zircons largely overlap with the K-N-E crustal evolution trend (TDM_2 ages > 2. 20 Ga), indicating a period of magma generation dominated by the reworking of ENMC crust or the contamination of juvenile mantle-derived magmas by ENMC crust. Post-1.45 Ga zircons display a more sawtooth-shaped evolution trend, with nearly half of the zircons plotting above the K-N-E crustal evolution trend (Fig. 13). The heterogeneous Nd isotopic composition of KC anorthosite and Red Granite further supports a crustal–mantle mixing model, with $\varepsilon Nd_{(i)}$ ranging from −12.7 to + 6.3 (Baxe, 2007; Drüppel et al., 2007; Gleißner et al., 2011; Mayer et al., 2004; Slejko et al., 2002).

The geodynamic setting for massif-type Proterozoic anorthosite generation is debated worldwide (e.g., Ashwal and Bybee, 2017; Roberts et al., 2023; and references therein), because these rocks do not exist on modern or Phanerozoic Earth and hence uniformitarianism cannot be applied. The Kunene Complex (1.50–1.36 Ga) has been interpreted as formed in an intraplate extensional setting related to a crustal thermal anomaly caused by ponding of mantle-derived melts at the base of the lithosphere (Brandt et al., 2003, 2007, 2021; Drüppel et al., 2007; Maier et al., 2013; Mayer et al., 2004). However, whereas the juvenile isotopic signature of the pre-KC ~ 1.56–1.50 Ga detrital and igneous zircons might be consistent with an intracontinental anorogenic setting, the mixed crustal–mantle Hf and Nd isotopic compositions of the KC magmatism are hard to reconcile with such a tectonic scenario. If KC magmatism was emplaced during long-lived (~140 Myr) intracontinental extension, an increased radiogenic signature would be expected over time in the KC magmatic products, reflecting an increased mantle input during progressive crustal thinning (e.g., Roberts and Spencer, 2015). Instead, the mixed isotopic signature of the KC may be explained by formation in a wide back-arc region of a long-lived accretionary orogen, with fluctuations in isotopic composition related to episodes of crustal thickening and lithospheric extension, as recently proposed for the Kunene Complex (Milani et al., 2022) and worldwide for massif-type Proterozoic anorthosites (Roberts et al., 2023 and references therein).

5.3.3.2. Post-KC magmatism and sedimentation (1.35–1.07 Ga). The U-Pb detrital zircon record of the Mesoproterozoic strata (~1.36–1.30 Ga) shows a predominant post-KC peak at ~ 1.35 Ga, with a younging tail to ~ 1.30 Ga (Fig. 10A), which corresponds to a relatively small peak in the magmatic record at ~ 1.33 Ga (Fig. 10B). This time period is characterized by the ~ 1.34–1.32 Ga Orue Unit anatectic event at upper-amphibolite facies metamorphism conditions (Brandt et al., 2021; Brandt and Klemd, 2008; Seth et al., 2005), as well as minor granitoid magmatism at ~ 1.35–1.34 Ga in the EMNC (Kröner and Rojas-Agramonte, 2017). Compared to the ~ 1.45–1.36 Ga period of KC magmatism, detrital zircon from the ~ 1.36–1.30 Ga period shows a significant increase in juvenile contribution (Fig. 13). Approximately 70 % of these zircons plot above the K-N-E crustal evolution trend (TDM_2 ages < 2.20 Ga), suggesting a renewed input from the depleted mantle or reworking of the earlier ~ 1.56–1.50 Ga juvenile crust.

The Orue metamorphic event has been linked to heat input from the KC (Brandt et al., 2021; Brandt and Klemd, 2008). The proposed clockwise P–T path is interpreted to reflect crustal thickening related to emplacement of KC magmas, followed by decompression during collapse of the magmatically thickened crust and rebound of the asthenospheric mantle under thinning lithosphere (Brandt et al., 2021). This may be consistent with the more radiogenic Hf isotopic composition of the ~ 1.36–1.30 Ga detrital zircons. However, as noted by Seth et al. (2005), the Orue event took place ~ 20 to 40 Myr after KC magmatism, making it unlikely that it is related to KC contact metamorphism. The cause of the Orue event remains undetermined; however, it may be linked to partial melting of the ENMC and juvenile crustal components dating from approximately 1.56 to 1.50 Ga due to asthenospheric mantle upwelling following the extensional collapse of a magmatically-thickened crust during an orogenic event. Alternatively, the juvenile magmatism could be associated with a new phase of slab retreat and the subsequent extension of the back-arc region within the accretionary margin setting proposed to have existed during KC magmatism.

Following Orue metamorphism and coeval magmatism, the southwest AS records the deposition of the Iona Group and Okapuka Formation sediments at ca. 1.32 Ga. These sedimentary units were later crosscut by ~ 1.29–1.18 Ga granitoids and felsic volcanics, nepheline syenites and carbonatites (main peak at ~ 1.23–1.22 Ga; Fig. 10; Kröner and Rojas-Agramonte, 2017; Simon et al., 2017; Tshiningayamwe et al., 2022; this study). Detrital zircons related to this magmatism account for only 2 % of the whole detrital zircon dataset, and only 5 % of the Mesoproterozoic detrital zircon record, possibly indicating that the magmatic volume and/or zircon fertility were relatively minor (Fig. 10A). Nonetheless, their Hf isotopic compositions show a remarkable overlap with those of the ~ 1.25–1.22 Ga alkali-feldspar porphyritic granite-gneiss and rhyolitic porphyry in the Iona region (Figs. 11 and 13A). These magmatic and detrital zircons plot within the compositional field defined by the evolution of the earlier ~ 1.56–1.50 Ga juvenile detrital and magmatic zircons (Fig. 13A), suggesting two possibilities for the generation of the ~ 1.29–1.18 Ga magmatism: (i) reworking of the ~ 1.56–1.50 Ga juvenile crust, or (ii) mixing between ENMC-derived melts and mantle-derived juvenile melts. Magmatism between ~ 1.29–1.18 Ga is followed by a new taphrogenic event responsible for the deposition of the upper part of the Ompupa Group and the Cahama Formation after 1.18 Ga.

Undeformed mafic dikes and sills (~1.13–1.10 Ga) linked to the Umkondo large igneous province (Ernst et al., 2013; Salminen et al., 2018) extend across the region and cut through the Ompupa Group and Cahama Formation. These, along with felsic sills intruding the Okapuka Formation at ~ 1.07 Ga (Kröner and Rojas-Agramonte, 2017), mark the end of Mesoproterozoic magmatism in the southwest AS.

6. Conclusions

1) The extensive and generally undeformed siliciclastic outliers from the Ompupa Plateau, Cahama and Iona regions of the southwest Angolan Shield in Angola are Mesoproterozoic in age, challenging previous correlations with the Paleoproterozoic Chela Group of the Humpata Plateau. These sedimentary rocks are associated with two late Ectasian to early Stenian taphrogenic events. The first event, represented by the Iona Group (and the laterally correlative Okapuka Formation in northwest Namibia) occurred after the upper-amphibolite facies metamorphism recorded in the Orue Unit of the ENMC (~1.34–1.32 Ga) and prior to granite intrusion into the Iona Group at ~ 1.25–1.22 Ga. The second event, represented by the Ompupa Group and the Cahama Formation, is bracketed between the latter magmatic event and the ~ 1.13–1.11 Ga mafic sills and dikes related to the Umkondo large igneous province.
2) U-Pb and Lu-Hf isotopes in detrital zircons reveal a pronounced similarity with the compiled data for magmatic rocks from the southwest Angolan Shield, suggesting that the source of the Mesoproterozoic siliciclastic rocks is pre-

dominantly internal to the Angolan Shield, with minimal external contributions. The age spectra of coarse-grained sandstones from the northern Ompupa Plateau and the Cahama Formation indicate a limited source area and proximity to dominant ~ 1.56–1.30 Ga Mesoproterozoic and ~ 1.87–1.73 Ga K-N-E sources, respectively. Conversely, other samples exhibit a diverse and heterogeneous distribution of detrital zircon ages, implying multiple sources, enhanced basin connectivity and a larger catchment area. Archean and Eburnean detrital zircons are likely sourced from the CEZ and Cassinga Zone in southern Angola and the Sesfontein-Grootfontein-Tsumkwe-Quangwadum inliers in northern Namibia. Paleoproterozoic K-N-E-age zircons are traced to the ENMC and the Kamanjab Inlier, whereas Mesoproterozoic zircons are attributed to the KC and, to a lesser extent, to pre- to post-KC intrusions in the ENMC.

3) Combining U-Pb and Lu-Hf isotopes for detrital and igneous zircon, along with whole-rock Sm-Nd isotopes, reveals significant temporal and spatial isotopic heterogeneities in the crustal evolution of the southwest Angolan Shield. Rare Archean to early Siderian detrital zircons display predominantly subchondritic Hf compositions. $\varepsilon Hf_{(i)}$ decreases with younging U-Pb ages and indicates successive reworking of a Paleo- to Mesoarchean crust. The basement of the southwest AS is dominated by Paleoproterozoic granitoids formed between ~ 2.05 and 1.73 Ga, delineating a two-stage Paleoproterozoic magmatic evolution. Eburnean magmatism (~2.05–1.93 Ga) is characterized by strongly negative Hf and Nd compositions, indicating predominant reworking of a pre-existing Archean crust, probably in a collisional orogenic setting. In contrast, K-N-E magmatism (1.87–1.73 Ga) displays an excursion towards more radiogenic Hf and Nd isotopic compositions, with an increasing juvenile component with decreasing age. K-N-E magmatism likely originated in an extensional accretionary orogen along the southern margin of the Eburnean-Archean crust of the southwest AS.

Following a ~ 200 Myr period of magmatic quiescence, activity in the southwest Angolan Shield resumed in the Mesoproterozoic at ~ 1.56 Ga and persisted until ~ 1.07 Ga. ~ 1.56 to 1.50 Ga magmatism is characterized by suprachondritic Hf and Nd compositions, indicating significant juvenile addition. Magmatism associated with the KC (~1.50–1.36 Ga) is marked by a large variation in Hf and Nd isotopic compositions, from highly evolved to moderately juvenile, consistent with variable mixing between reworked ENMC-crust and juvenile melts. The temporally variable and mixed isotopic signature of KC magmas was possibly generated in a wide back-arc region, suggesting a long-lived accretionary orogen along an active continental margin of the southwestern AS, as recently suggested for Proterozoic massif-type anorthosites elsewhere.

The Hf isotopic record of post-KC (~1.36–1.30 Ga) detrital zircons indicates a greater juvenile contribution compared to KC magmatism. This shift might be related to a renewed phase of slab retreat and associated extension of the back-arc region or asthenospheric mantle upwelling following extensional collapse of the magmatically-thickened crust during an orogenic event. A subsequent episode of magmatism from ~ 1.29 to 1.18 Ga displays Hf isotopic compositions that overlap with the crustal evolution trend of the earlier ~ 1.56 to 1.50 Ga juvenile magmatism. This suggests: (i) reworking of ~ 1.56 to 1.50 Ga juvenile crust; or (ii) mixing between ENMC crust and mantle-derived juvenile melts. The emplacement of regionally extensive undeformed ~ 1.13 and 1.10 Ga mafic dikes and sills of the Umkondo large igneous province in the Ompupa Group and Cahama Formation, together with ~ 1.07 Ga felsic sills intrusive into the Okapuka Formation, marks the end of Mesoproterozoic magmatism in the southwest AS.

CRediT authorship contribution statement

Ezequiel Ferreira: Conceptualization, Investigation, Formal analysis, Validation, Visualization, Data curation, Writing – original draft. **Jérémie Lehmann:** Conceptualization, Investigation, Visualization, Supervision, Resources, Writing – review & editing. **José Feliciano Rodrigues:** Resources, Supervision, Writing – review & editing. **Ben Hayes:** Investigation, Writing – review & editing. **Enrique Merino-Martínez:** Writing – review & editing. **Lorenzo Milani:** Writing – review & editing. **Grant M. Bybee:** Writing – review & editing. **Trishya M. Owen Smith:** Writing – review & editing. **José Luis García-Lobón:** . **Colombo C. G. Tassinari:** Methodology, Resources, Writing – review & editing. **Henriette Ueckermann:** Methodology, Validation. **Kei Sato:** Methodology, Validation. **Paulo Bravo Silva:** Investigation, Resources. **João Correia:** Resources. **José Labaredas:** Resources. **Laurent Duarte:** Resources. **Mmasetena Anna Molekwa:** Investigation. **José Manuel:** Resources. **Américo da Mata Lourenço Victorino:** Resources.

Declaration of competing interest

The authors declare that they have no known competing financial interests or personal relationships that could have appeared to influence the work reported in this paper.

Acknowledgements

Ezequiel Ferreira and Jeremie Lehmann are grateful to Eurico Pereira and Hielke Jelsma for the insightful discussions about the geology of southwest Angola. The authors thank Reuben Ngobeli (University of Johannesburg) for his assistance with zircon separation and cathodoluminescence imaging of the sedimentary samples, and Artur Onoe (University of São Paulo) for his assistance with zircon cathodoluminescence imaging of the igneous samples. We also thank Andreas Gaertner and an anonymous reviewer for their valuable comments and Andrea Festa for the efficient editorial handling of the manuscript.Ferreira's research visit to the University of Johannesburg and the analysis of sedimentary samples were funded by the PPM Research Group (University of Johannesburg). Funding for the analysis of igneous samples was provided by the PLANAGEO program. The support of the DSI-NRF Centre of Excellence (CoE) for Integrated Mineral and Energy Resource Analysis (DSI-NRF CIMERA) and Anglo American towards this research are acknowledged. This publication is part of the Angolan government-sponsored geological mapping program (PLANAGEO), implemented by the Geological Survey of Angola (IGEO) under the supervision of the Angolan Ministry of Mineral Resources, Petroleum, and Gas (MIREMPET).

Appendix A. Supplementary material

Supplementary data to this article can be found online at https://doi.org/10.1016/j.gr.2024.03.010.

References

Andersen, T., Andersson, U., Graham, S., Åberg, G., Simonsen, S., 2009. Granitic magmatism by melting of juvenile continental crust: new constraints on the source of palaeoproterozoic granitoids in fennoscandia from hf isotopes in zircon. J. Geol. Soc. London 166, 233–247. https://doi.org/10.1144/0016-76492007-166.

Andersen, T., Elburg, M., Cawthorn-Blazeby, A., 2016a. U-pb and Lu–Hf zircon data in young sediments reflect sedimentary recycling in eastern South Africa. J. Geol. Soc. London 173, 337–351. https://doi.org/10.1144/jgs2015-006.

Andersen, T., Griffin, W., 2004. Lu–Hf and U-pb isotope systematics of zircons from the storgangen intrusion, Rogaland intrusive complex, SW Norway: implications for the composition and evolution of precambrian lower crust in

the Baltic shield. Lithos 73, 271–288. https://doi.org/10.1016/j.lithos.2003.12.010.
Andersen, T., Saeed, A., Gabrielsen, A.R., Olaussen, S., 2011. Provenance characteristics of the Brumunddal sandstone in the Oslo rift derived from U-pb, lu-hf and trace element analyses of detrital zircons by laser ablation ICMPS. Norw. J. Geol. 91, 1–18.
Andersen, T., Kristoffersen, M., Elburg, M., 2016b. How far can we trust provenance and crustal evolution information from detrital zircons? a south african case study. Gondwana Res. 34, 129–148. https://doi.org/10.1016/j.gr.2016.03.003.
Andersen, T., Kristoffersen, M., Elburg, M., 2018. Visualizing, interpreting and comparing detrital zircon age and hf isotope data in basin analysis - a graphical approach. Basin Res. 30, 132–147. https://doi.org/10.1111/bre.12245.
Ashwal, L.D., Bybee, G.M., 2017. Crustal evolution and the temporality of anorthosites. Earth Sci. Rev. 173, 307–330. https://doi.org/10.1016/j.earscirev.2017.09.002.
Baxe, O., 2007. Geocronologia de complexos máfico-ultramáficos: exemplo da série superior do Complexo de Niquelândia, brasil, e do Complexo do Kunene. Universidade de Brasília. Angola MSc thesis.
Beetz, P., 1933. Geology of south West Angola, between Cunene and lunda Axis. Trans. r. Soc. s. Afr. 36, 137–176.
Belousova, E.A., Kostitsyn, Y.A., Griffin, W.L., Begg, G.C., O'Reilly, S.Y., Pearson, N.J., 2010. The growth of the continental crust: constraints from zircon hf-isotope data. Lithos 119, 457–466. https://doi.org/10.1016/j.lithos.2010.07.024.
Bouvier, A., Vervoort, J., Patchett, P.J., 2008. The Lu–Hf and Sm–Nd isotopic composition of CHUR: constraints from unequilibrated chondrites and implications for the bulk composition of terrestrial planets. Earth Planet. Sci. Lett. 273, 48–57. https://doi.org/10.1016/j.epsl.2008.06.010.
Brandt, S., Klemd, R., 2008. Upper-amphibolite facies partial melting of paragneisses from the epupa complex, NW Namibia, and relations to mesoproterozoic anorthosite magmatism. J. Metamorph. Geol. 26, 871–893. https://doi.org/10.1111/j.1525-1314.2008.00793.x.
Brandt, S., Klemd, R., Okrusch, M., 2003. Ultrahigh-temperature metamorphism and multistage evolution of Garnet-orthopyroxene granulites from the proterozoic epupa complex, NW Namibia. J. Petrol. 44, 1121–1144. https://doi.org/10.1093/petrology/44.6.1121.
Brandt, S., Will, T., Klemd, R., 2007. Magmatic loading in the proterozoic epupa complex, NW Namibia, as evidenced by ultrahigh-temperature sapphirine-bearing orthopyroxene–sillimanite–quartz granulites. Precambrian Res. 153, 143–178. https://doi.org/10.1016/j.precamres.2006.11.016.
Brandt, S., Klemd, R., Xie, H., Bobek, P., 2021. Unravelling the P-T-t history of three high-grade metamorphic events in the epupa complex, NW Namibia: implications for the paleoproterozoic to mesoproterozoic evolution of the Congo craton. Am. J. Sci. 321, 235–296. https://doi.org/10.2475/01.2021.07.
Bravo Silva, P., Oliveira, A., Duarte, L., Labaredas, J., Goicoechea, P., 2021. Carta Geológica de Angola à escala 1:250 000, folha Sul D-33/T (Chibia) e memória explicativa (2a edição). UTE (IGME, LNEG, Impulso) – IGEO, Luanda, 225 pp.
Buzzi Marcos, J., Gutiérrez-Medina, M., 2021. Carta Geológica de Angola à escala 1:250.000, folha Sul D-33/X (Cassinga) e memória explicativa. UTE (IGME, LNEG, Impulso) – IGEO, Luanda, 152 pp.
Bybee, G.M., Hayes, B., Owen-Smith, T.M., Lehmann, J., Ashwal, L.D., Brower, A.M., Hill, C.M., Corfu, F., Manga, M., 2019. Proterozoic massif-type anorthosites as the archetypes of long-lived (≥100 myr) magmatic systems—New evidence from the Kunene Anorthosite complex (Angola). Precambrian Res. 332. https://doi.org/10.1016/j.precamres.2019.105393.
Campeny, M., Proenza, J.A., Castillo-Oliver, M., Torró, L., Villanova-de-Benavent, C., Melgarejo, J., Gonçalves, A., Román-Alpiste, M., Blanco-Quintero, I., Llovet, X., Farré-de-Pablo, J., 2023. Petrology, metallogeny and U-pb geochronology of the paleoproterozoic mafic-ultramafic hamutenha intrusion. Angolan Shield. J. Afr. Earth. Sci. 197. https://doi.org/10.1016/j.jafrearsci.2022.104733.
Capaldi, T.N., McKenzie, N.R., Horton, B.K., Mackaman-Lofland, C., Colleps, C.L., Stockli, D.F., 2021. Detrital zircon record of phanerozoic magmatism in the southern Central Andes. Geosphere 17, 876–897. https://doi.org/10.1130/GES02346.1.
Carvalho, H., 1969. Cronologia das formações geológicas precâmbricas na região central do sudoeste de Angola e tentativa de correlação com as do sudoeste africano. Serv. Geol. Min. Angola 20, 61–71.
Carvalho, H., 1972. Chronologie des formations géologiques précambriennes de la région Centrale du Sud-Ouest de l'Angola et essai de corrélation avec celles du Sud-oest africain. 24th int. Geol. Congr. 1, 187–194.
Carvalho, H., 1984. Estratigrafia do precâmbrico de Angola. sep. Garcia de orta. Sér. Geol. 7, 1–66.
Carvalho, H., Alves, P., 1993. The precambrian of SW Angola and NW Namibia. general Remarks. Correlation analysis. economic geology. Comun. Inst. Invest. Cient. Trop. 4, 1–38.
Carvalho, H., Simões, M., 1971. Notícia explicativa da carta geológica de Angola, folha 376 (Macota), escala 1:100.000. Dir. Prov. Serv. Geol. Minas Angola, Luanda.
Carvalho, H., Crasto, J.P., Silva, Z.C.G., Viaiette, Y., 1987. The Kibaran cycle in Angola-a discussion. Geol. J. 22, 85–102.
Carvalho, H., Simões, M., 1972. Algumas considerações sobre as séries metamórficas da região central do sudoeste de Angola. Separ. Rev. Fac. Ciênc. Lisboa XVII, 135–158.
Carvalho, H., Tassinari, C., Alves, P.H., Guimarães, F., Simões, M.C., 2000. Geochronological review of the precambrian in western Angola: links with Brazil. J. Afr. Earth. Sci. 31, 383–402. https://doi.org/10.1016/S0899-5362(00)00095-6.
Carvalho, H., 1981. Geologia de Angola (folhas 1, 2, 3 e 4; escala 1/1.000.000), Inst. Inv. Cient. Tropical, Lisboa.
Chapman, J.B., Ducea, M.N., Kapp, P., Gehrels, G.E., DeCelles, P.G., 2017. Spatial and temporal radiogenic isotopic trends of magmatism in cordilleran orogens. Gondwana Res. 48, 189–204. https://doi.org/10.1016/j.gr.2017.04.019.
Chu, Y., Lin, W., Faure, M., Wang, Q., 2016. Detrital zircon U-pb ages and hf isotopic constraints on the terrigenous sediments of the Western Alps and their paleogeographic implications. Tectonics 35, 2734–2753. https://doi.org/10.1002/2016TC004276.
Collins, W., Belousova, E., Kemp, A., Murphy, J.B., 2011. Two contrasting phanerozoic orogenic systems revealed by hafnium isotope data. Nat. Geosci. 4, 333–337. https://doi.org/10.1038/ngeo1127.
Correia, H., 1976. O grupo chela e a formação leba como novas unidades litoestratigráfics resultantes da redefinição da formação da chela na região do planalto da Humpata (sudoeste de Angola). Bol. Soc. Geol. Portugal 20, 65–130.
Coutts, D., Matthews, W., Hubbard, S., 2019. Assessment of widely used methods to derive depositional ages from detrital zircon populations. Geosci. Front. 10, 1421–1435. https://doi.org/10.1016/j.gsf.2018.11.002.
Dickinson, W.R., Gehrels, G.E., 2009. Use of U-pb ages of detrital zircons to infer maximum depositional ages of strata: a test against a Colorado plateau mesozoic database. Earth Planet. Sci. Lett. 288, 115–125. https://doi.org/10.1016/j.epsl.2009.09.013.
Drüppel, K., Littmann, S., Romer, R.L., Okrusch, M., 2007. Petrology and isotope geochemistry of the mesoproterozoic anorthosite and related rocks of the Kunene intrusive complex. NW Namibia. Precambrian Res. 156, 1–31. https://doi.org/10.1016/j.precamres.2007.02.005.
Ernst, R., Pereira, E., Hamilton, M., Pisarevsky, S., Rodriques, J., Tassinari, C., Teixeira, W., Van-Dunem, V., 2013. Mesoproterozoic intraplate magmatic "barcode" record of the Angola portion of the Congo craton: newly dated magmatic events at 1505 and 1110Ma and implications for nuna (Columbia) supercontinent reconstructions. Precambrian Res. 230, 103–118. https://doi.org/10.1016/j.precamres.2013.01.010.
Escuder-Viruete, J., Gumiel, J., 2021. Carta Geológica de Angola à escala 1:250.000, folha Sul E-33/C e Sul E-33/I (Cahama) e memória explicativa. UTE (IGME, LNEG, Impulso) – IGEO, Luanda, 249 pp.
Escuder-Viruete, J., Correia, J., Quintana, L., Gumiel, J., Merino-Martínez, E., 2021a. Carta Geológica de Angola à escala 1:250.000, folha Sul D-33/S (Namibe) e memória explicativa. UTE (IGME, LNEG, Impulso) – IGEO, Luanda, 199 pp.
Escuder-Viruete, J., Merino-Martínez, E., González, P., Quintana, L., Duarte, L., Goicoechea, P., 2021b. Carta Geológica de Angola à escala 1:250.000, folha Sul E-33/B e Sul E-33/H (Oncócua) e memória explicativa. UTE (IGME, LNEG, Impulso) – IGEO, Luanda, 173 pp.
Franz, L., Romer, R., Dingeldey, D., 1999. Diachronous Pan-african granulite-facies metamorphism (650 ma and 550 ma) in the Kaoko Belt, NW Namibia. Eur. J. Mineral. 11, 167–180.
Galán, G., 2021. Carta Geológica de Angola à escala 1:250.000, folha Sul D-33/O (Quipungo) e memória explicativa. UTE (IGME, LNEG, Impulso) – IGEO, Luanda, 194 pp.
Gärtner, A., Hofmann, M., Zieger, J., Sagawe, A., Krause, R., Stutzriemer, M., Gesang, S., Gerdes, A., Marko, L., Lana, C., Linnemann, U., 2022. Implications for sedimentary transport processes in southwestern Africa: a combined zircon morphology and age study including extensive geochronology databases. Int. J. Earth Sci. 111, 767–788. https://doi.org/10.1007/s00531-021-02146-1.
Gehrels, G., 2014. Detrital zircon U-pb geochronology applied to tectonics. Annu. Rev. Earth Planet. Sci. 42, 127–149. https://doi.org/10.1146/annurev-earth-050212-124012.
Gleißner, P., Drüppel, K., Romer, R., 2011. The role of crustal contamination in massif-type anorthosites, new evidence from Sr–Nd–Pb isotopic composition of the Kunene intrusive complex. NW Namibia. Precambrian Res. 185, 18–36. https://doi.org/10.1016/j.precamres.2010.11.004.
Goscombe, B., Gray, D., Armstrong, R., Foster, D., Vogl, J., 2005. Event geochronology of the Pan-african Kaoko Belt. Namibia. Precambrian Res. 140, 103.e1–103.e41. https://doi.org/10.1016/j.precamres.2005.07.003.
Griffin, W., Pearson, N., Belousova, E., Jackson, S., van Achterbergh, E., O'Reilly, S.Y., Shee, S., 2000. The hf isotope composition of cratonic mantle: LAM-MC-ICPMS analysis of zircon megacrysts in kimberlites. Geochim. Cosmochim. Acta 64, 133–147. https://doi.org/10.1016/S0016-7037(99)00343-9.
Griffin, W.L., Wang, X., Jackson, S.E., Pearson, N.J., O'Reilly, S., Xu, X., Zhou, X., 2002. Zircon chemistry and magma mixing, SE China: in-situ analysis of hf isotopes, tonglu and pingtan igneous complexes. Lithos 61, 237–269. https://doi.org/10.1016/S0024-4937(02)00082-8.
Gumiel, J., Martín-Banda, R., Iglesias-Martínez, M., Goicoechea, P., 2021. Carta Geológica de Angola à escala 1:250.000, folha Sul E-33/D e Sul E-33/J (Ondjiva) e memória explicativa. UTE (IGME, LNEG, Impulso) – IGEO, Luanda, 203 pp.
Gutiérrez-Medina, M., Chamizo-Borreguero, M., Ponde Escudero, C., 2021. Carta Geológica de Angola à escala 1:250.000, folha Sul D-33/M (Munhino) e memória explicativa. UTE (IGME, LNEG, Impulso) – IGEO, Luanda, 236 pp.
Guynn, J., Gehrels, G., 2010. Comparison of detrital zircon age distributions using the K-S test, Arizona LaserChron center. University of Arizona. https://sites.google.com/laserchron.org/arizonalaserchroncenter/home.
Hall, W., Hitzman, M., Kuiper, Y., Kylander-Clark, A., Holm-Denoma, C., Moscati, R., Plink-Björklund, P., Enders, M.S., 2018. Igneous and detrital zircon U-pb and lu-hf geochronology of the late meso- to neoproterozoic northwest Botswana rift: maximum depositional age and provenance of the Ghanzi group, Kalahari Copperbelt. Botswana and Namibia. Precambrian Res. 318, 133–155. https://doi.org/10.1016/j.precamres.2018.10.001.

Hayes, B., Lehmann, J., Bybee, G., Owen-Smith, T., 2022. Crystal transfer from magma to wallrock during syntectonic granite emplacement. J. Geol. Soc. London. 179. https://doi.org/10.1144/jgs2020-125.
Heinonen, A.P., Andersen, T., Rämö, O.T., 2010. Re-evaluation of rapakivi petrogenesis: source constraints from the hf isotope composition of zircon in the rapakivi granites and associated mafic rocks of southern Finland. J. Petrol. 51, 1687–1709. https://doi.org/10.1093/petrology/egq035.
Hoal, K., Hoal, B., Griffin, W., Armstrong, R., 2000. Characterization of the age and nature of the lithosphere in the tsumkwe region Namibia. Communs Geol. Surv. Namibia 12, 23–30.
Hoskin, P., 2003. The composition of zircon and igneous and metamorphic petrogenesis. Rev. Mineral. Geochem. 53, 27–62. https://doi.org/10.2113/0530027.
Hoskin, P., Black, L., 2000. Metamorphic zircon formation by solid-state recrystallization of protolith igneous zircon. J. Metamorph. Geol. 18, 423–439. https://doi.org/10.1046/j.1525-1314.2000.00266.x.
Janoušek, V., Konopásek, J., Ulrich, S., Erban, V., Tajčmanová, L., Jeřábek, P., 2010. Geochemical character and petrogenesis of Pan-african amspoort suite of the Boundary igneous complex in the Kaoko Belt (NW Namibia). Gondwana Res. 18, 688–707. https://doi.org/10.1016/j.gr.2010.02.014.
Jelsma, H.A., McCourt, S., Perritt, S.H. and Armstrong, R.A. 2018. The geology and evolution of the Angolan shield, Congo craton. In: Siegesmund S., Basei M., Oyhantçabal P., and Oriolo S. (Eds.), Geology of Southwest Gondwana. Regional Geology Reviews. Springer, Cham, 217–239,. Doi: 10.1007/978-3-319-68920-3_9.
Jung, S., Mezger, K., Nebel, O., Kooijman, E., Berndt, J., Hauff, F., Münker, C., 2012. Origin of meso-proterozoic post-collisional leucogranite suites (kaokoveld, Namibia): constraints from geochronology and nd, sr, hf, and pb isotopes. Contrib. Mineral. Petrol. 163, 1–17. https://doi.org/10.1007/s00410-011-0655-y.
Kemp, A.I.S., Hawkesworth, C.J., Collins, W.J., Gray, C.M., Blevin, P.L., 2009. Isotopic evidence for rapid continental growth in an extensional accretionary orogen: the tasmanides, eastern Australia. Earth Planet. Sci. Lett. 284, 455–466. https://doi.org/10.1016/j.epsl.2009.05.011.
Kleinhanns, I.C., Fullgraf, T., Wilsky, F., Nolte, N., Fliegel, D., Klemd, R., Hansen, B.T., 2013. U-pb zircon ages and (isotope) geochemical signatures of the kamanjab inlier (NW Namibia): constraints on palaeoproterozoic crustal evolution along the southern Congo craton. Geol. Soc. Spec. Publ. 389, 165–195. https://doi.org/10.1144/SP389.1.
Kohanpour, F., Kirkland, C., Gorczyk, W., Occhipinti, S., Lindsay, M., Mole, D., Le Vaillant, M., 2019. Hf isotopic fingerprinting of geodynamic settings: integrating isotopes and numerical models. Gondwana Res. 73, 190–199. https://doi.org/10.1016/j.gr.2019.03.017.
Kröner, A., Correia, H., 1980. Continuation of the Pan-african Damara belt into Angola: a proposed correlation of the chela group in southern Angola with the nosib group in northern namibia/South West Africa. Trans. Geol. Soc. s. Afr. 83, 5–16.
Kröner, S., Konopásek, J., Kröner, A., Passchier, C., Poller, U., Wingate, M., Hofmann, K., 2004. U-pb and pb-pb zircon ages for metamorphic rocks in the Kaoko Belt of northwestern Namibia: a palaeo- to mesoproterozoic basement reworked during the Pan-african orogeny. S. Afr. J. Geol. 107, 455–476.
Kröner, A., Rojas-Agramonte, Y., 2017. Mesoproterozoic (Grenville-age) granitoids and supracrustal rocks in kaokoland, northwestern Namibia. Precambrian Res. 298, 572–592. https://doi.org/10.1016/j.precamres.2017.07.008.
Kröner, A., Rojas-Agramonte, Y., Hegner, E., Hoffmann, K.H., Wingate, M.T.D., 2010. SHRIMP zircon dating and nd isotopic systematics of palaeoproterozoic migmatitic orthogneisses in the epupa metamorphic complex of northwestern Namibia. Precambrian Res. 183, 50–69. https://doi.org/10.1016/j.precamres.2010.06.018.
Kröner, A., Rojas-Agramonte, Y., Wong, J., Wilde, S.A., 2015. Zircon reconnaissance dating of proterozoic gneisses along the Kunene River of northwestern Namibia. Tectonophysics 662, 125–139. https://doi.org/10.1016/j.tecto.2015.04.020.
Kröner, S., 2005. Geochronological and Structural Evolution of the Western and Central Kaoko Belt in NW Namibia (PhD thesis). Johannes Gutenberg-Universität Mainz, Mainz. Doi: http://doi.org/10.25358/openscience-1899.
Labaredas, J., Correia, J., Rodrigues, J.F., 2021. Carta Geológica de Angola à escala 1:250.000, folha Sul E-33/A (Espinheira) e memória explicativa. UTE (IGME, LNEG, Impulso) – IGEO, Luanda, 324 pp.
Langa, W.M., 2019. The petrology and economic potential of mafic-ultramafic intrusions west of the Kunene Anorthosite complex, SW Angola (MSc dissertation). University of Johannesburg, Johannesburg. https://hdl.handle.net/10210/417486.
Lehmann, J., Bybee, G.M., Hayes, B., Owen-Smith, T.M., Belyanin, G., 2020. Emplacement of the giant Kunene AMCG complex into a contractional ductile shear zone and implications for the mesoproterozoic tectonic evolution of SW Angola. Int. J. Earth Sci. 109, 1463–1485. https://doi.org/10.1007/s00531-020-01837-5.
Lehmann, J., Brower, A., Owen-Smith, T., Bybee, G., Hayes, B., 2023. Landsat 8 and alos DEM geological mapping reveals the architecture of the giant mesoproterozoic Kunene complex anorthosite suite (Angola/Namibia). Geosci. Front. 14,. https://doi.org/10.1016/j.gsf.2023.101620 101620.
Li, X.-H., Li, Z.-X., Li, W.-X., 2014. Detrital zircon U-pb age and hf isotope constrains on the generation and reworking of precambrian continental crust in the cathaysia block. South China: A Synthesis. Gondwana Res. 25, 1202–1215. https://doi.org/10.1016/j.gr.2014.01.003.
Littmann, S., Romer, R., Okrusch, M., 2000. Nephelinsyenite der epembe-Swartbooisdrif-alkali-provinz (ESAP)/NW-Namibia. DMG. Beih. Eur. J. Mineral. 12.
Lloyd, J., Collins, A., Payne, J., Glorie, S., Holford, S., Reid, A., 2016. Tracking the cretaceous transcontinental Ceduna River through Australia: the hafnium isotope record of detrital zircons from offshore southern Australia. Geosci. Front. 7, 237–244. https://doi.org/10.1016/j.gsf.2015.06.001.
Ludwig, K., 1998. On the treatment of concordant uranium-Lead ages. Geochim. Cosmochim. Acta 62, 665–676. https://doi.org/10.1016/S0016-7037(98)00059-3.
Ludwig, K.R., 2012. User's manual for isoplot version 3.75–4.15: a geochronological toolkit for Microsoft excel. Berkeley Geochronol. Cent. Spec. Publ. 5.
Luft, J.L., Chemale, F., Armstrong, R., 2011. Evidence of 1.7- to 1.8-ga collisional arc in the Kaoko Belt. NW Namibia. Int. J. Earth Sci. 100, 305–321. https://doi.org/10.1007/s00531-010-0591-5.
Maier, W.D., Rasmussen, B., Fletcher, I.R., Li, C., Barnes, S.-J., Huhma, H., 2013. The Kunene Anorthosite complex, Namibia, and its satellite intrusions: geochemistry, geochronology, and economic potential. Econ. Geol. 108, 953–986. https://doi.org/10.2113/econgeo.108.5.953.
Máximo, J., Sousa, J.C., Oliveira, A., 2021a. Carta Geológica de Angola à escala 1:250.000, folha Sul D-33/V (Cuvelai) e memória explicativa. UTE (IGME, LNEG, Impulso) – IGEO, Luanda, 211 pp.
Máximo, J., Sousa, J.C., Oliveira, A., 2021b. Carta Geológica de Angola à escala 1:250.000, folha Sul D-33/Q (Jamba) e memória explicativa. UTE (IGME, LNEG, Impulso) – IGEO, Luanda, 257 pp.
Mayer, A., Hofmann, A.W., Sinigoi, S., Morais, E., 2004. Mesoproterozoic sm-nd and U-pb ages for the Kunene Anorthosite complex of SW Angola. Precambrian Res. 133, 187–206. https://doi.org/10.1016/j.precamres.2004.04.003.
McCourt, S., Armstrong, R.A., Jelsma, H., Mapeo, R.B.M., 2013. New U-pb SHRIMP ages from the Lubango region, SW Angola: insights into the palaeoproterozoic evolution of the angolan shield, southern Congo craton. Africa. J. Geol. Soc. London 170, 353–363. https://doi.org/10.1144/jgs2012-059.
Merino-Martínez, E., Goicoechea, P., 2021. Carta Geológica de Angola à escala 1:250.000, folha Sul D-33/N (Lubango) e memória explicativa. UTE (IGME, LNEG, Impulso) – IGEO, Luanda, 324 pp.
Merino-Martínez, E., Rodrigues, J.F., Ferreira, E., 2021. In: Mapa Geológico De Angola à Escala 1:1.000.000 e Notícia Explicativa, p. 242 pp..
Milani, L., Lehmann, J., Bybee, G.M., Owen-Smith, T.M., Oosthuizen, L., Delport, P., Ueckermann, H., 2022. Geochemical and geochronological constraints on the mesoproterozoic red granite suite, Kunene AMCG complex of Angola and Namibia. Precambrian Res. 379.
Mouta, F., 1954. Notícia explicativa do esboço geológico de Angola (1:2.000.000). Junta Invest. Ultramar, Lisboa,
Pereira, E., Tassinari, C.C.G., Rodrigues, J.F., Van-Dúnem, M.V., 2011. New data on the deposition age of the volcano-sedimentary chela group and its eburnean basement: implications to post-eburnean crustal evolution of the SW of Angola. Commun. Geol. 98, 29–40.
Peucat, J., Vidal, P., Bernard-Griffiths, J., Condie, K., 1989. Sr, nd, and pb isotopic systematics in the archean low- to high-grade transition zone of southern India: syn-accretion vs. Post-Accretion Granulites. J. Geol. 97, 537–549. https://doi.org/10.1086/629333.
Potti, J.M., 2021. Carta Geológica de Angola à escala 1:250.000, folha Sul D-33/P (Matala) e memória explicativa. UTE (IGME, LNEG, Impulso) – IGEO, Luanda, 159 pp.
Rey-Moral, C., Mochales, T., Merino-Martínez, E., García Lobón, J.L., López Bahut, M. T., Martín-Banda, R., Feria, M.C., Ballesteros, D., Machadinho, A., Alves, D., 2022. Recording the largest gabbro-anorthositic complex worldwide: the Kunene complex (KC). SW Angola. Precambrian Res. 379,. https://doi.org/10.1016/j.precamres.2022.106790 106790.
Roberts, N., Condie, K., Palin, R., Spencer, C., 2023. Hot, wide, continental Back-arcs explain Earth's enigmatic mid-proterozoic magmatic and metamorphic record. Tektonika 1. https://doi.org/10.55575/tektonika2023.1.1.32.
Roberts, N.M.W., Spencer, C.J., 2015. The zircon archive of continent formation through time. Geol. Soc. Spec. Publ. 389, 197–225. https://doi.org/10.1144/SP389.14.
Rodrigues, J.F., Merino-Martínez, E., Ferreira, E., Francés, A., 2021b. Mapa Tectónico de Angola à escala 1:1.000.000 e notícia explicativa. UTE (IGME, LNEG, Impulso) – IGEO, Luanda, 106 pp.
Rodrigues, J.F., Ferreira, E., Merino-Martínez, E., Pereira, E., 2021. In: Mapa Geológico De Angola, Escala 1:500.000, Bloco UTE-1, p. 222 pp..
Rubatto, D., 2017. Zircon: the metamorphic mineral. Rev. Mineral. Geochem. 83, 261–295. https://doi.org/10.2138/rmg.2017.83.9.
Rudnick, R.L., Gao, S., 2014. Composition of the Continental Crust. In: Holland, H., Turekian, K. (Eds.), Treatise on Geochemistry (Second Edition). Elsevier, 1-51. Doi: 10.1016/B978-0-08-095975-7.00301-6.
Salminen, J., Hanson, R., Evans, D., Gong, Z., Larson, T., Walker, O., Gumsley, A., Söderlund, U., Ernst, R., 2018. Direct mesoproterozoic connection of the Congo and Kalahari cratons in proto-Africa: strange attractors across supercontinental cycles. Geology 46, 1011–1014. https://doi.org/10.1130/G45294.1.
Sanz, A.L.-G., 2005. Pre- and Post-Katangan Granitoids of the Greater Lufilian Arc - Geology, Geochemistry, Geochronology and Metallogenic Significance (PhD

thesis). University of the Witwatersrand, Johannesburg. http://hdl.handle.net/10539/4991.
Saylor, J., Jordan, J., Sundell, K., Wang, X., Wang, S., Deng, T., 2017. Topographic growth of the jishi Shan and its impact on basin and hydrology evolution. NE Tibetan Plateau. Basin Res. 30, 544–563. https://doi.org/10.1111/bre.12264.
Serv. Geol. Minas Angola, 1961. Notícia explicativa das folhas (provisórias) Sul E-33/A-G Iona e Sul E-33/B-C-H-I Oncócua da Carta Geológica de Angola à escala 1:250.000. Luanda.
Seth, B., 1999. Crustal evolution of the kaoko belt, NW Namibia. geochemical and geochronological study of archaean to mesoproterozoic basement gneisses and Pan-african migmatites and granitoids. Julius Maximilian University of Würzburg, Würzburg, Germany. PhD thesis)..
Seth, B., Kröner, A., Mezger, K., Nemchin, A.A., Pidgeon, R.T., Okrusch, M., 1998. Archaean to neoproterozoic magmatic events in the kaoko belt of NW Namibia and their geodynamic significance. Precambrian Res. 92, 341–363. https://doi.org/10.1016/S0301-9268(98)00086-2.
Seth, B., Armstrong, R., Brandt, S., Villa, I., Kramers, J., 2003. Mesoproterozoic U-pb and Pb–Pb ages of granulites in NW Namibia: reconstructing a complete orogenic cycle. Precambrian Res. 126, 147–168. https://doi.org/10.1016/S0301-9268(03)00193-1.
Seth, B., Armstrong, R., Büttner, A., Villa, I., 2005. Time constraints for mesoproterozoic upper amphibolite facies metamorphism in NW Namibia: a multi-isotopic approach. Earth Planet. Sci. Lett. 230, 355–378. https://doi.org/10.1016/j.epsl.2004.11.022.
Simon, S., Wei, C., Ellmies, R., Yang, H., Soh, T., 2017. New SIMS U-pb age on zircon from the epembe carbonatite dyke, NW Namibia: implications for mesoproterozoic evolution of carbonatites at the southern margin of the Congo craton. J. Afr. Earth. Sci. 135, 108–114. https://doi.org/10.1016/j.jafrearsci.2017.08.011.
Simpson, E., 1970. The anorthosite of southern Angola: a review of present data. In: Clifford, T., Gass, I. (Eds.), African Magmatism and Tectonics. Oliver and Boyd, Edinburgh, pp. 89–96.
Singletary, S., Hanson, R., Martin, M., Crowley, J., Bowring, S., Key, R., Ramokate, L., Direng, B., Krol, M., 2003. Geochronology of basement rocks in the Kalahari Desert, Botswana, and implications for regional proterozoic tectonics. Precambrian Res. 121, 47–71. https://doi.org/10.1016/S0301-9268(02)00201-2.
Slejko, F., Demarchi, G., Morais, E., 2002. Mineral chemistry and nd isotopic composition of two anorthositic rocks from the Kunene complex (South Western Angola). J. Afr. Earth. Sci. 35, 77–88. https://doi.org/10.1016/S0899-5362(02)00007-6.
Söderlund, U., Patchett, P., Vervoort, J., Isachsen, C., 2004. The 176Lu decay constant determined by Lu–Hf and U-pb isotope systematics of precambrian mafic intrusions. Earth Planet. Sci. Lett. 219, 311–324. https://doi.org/10.1016/S0012-821X(04)00012-3.
Spencer, C.J., Hawkesworth, C., Cawood, P.A., Dhuime, B., 2013. Not all supercontinents are created equal: Gondwana-rodinia case study. Geology 41, 795–798. https://doi.org/10.1130/G34520.1.
Spencer, C., Kirkland, C., 2016. Visualizing the sedimentary response through the orogenic cycle: a multidimensional scaling approach. Lithosphere 8 (1), 29–37. https://doi.org/10.1130/L479.1.
Spencer, C.J., Kirkland, C.L., Prave, A.R., Strachan, R.A., Pease, V., 2019. Crustal reworking and orogenic styles inferred from zircon hf isotopes: proterozoic examples from the North Atlantic region. Geosci. Front. 10, 417–424. https://doi.org/10.1016/j.gsf.2018.09.008.
Sundell, K.E., Macdonald, F.A., 2022. The tectonic context of hafnium isotopes in zircon. Earth Planet. Sci. Lett. 584,. https://doi.org/10.1016/j.epsl.2022.117426 117426.
Sundell, K., Saylor, J., Pecha, M., 2019. Provenance and recycling of detrital zircons from cenozoic altiplano strata and the crustal evolution of western South America from combined U-pb and lu-hf isotopic analysis. In: Horton, B.K., Folguera, A. (Eds.), Andean Tectonics. Elsevier, pp. 363–397. https://doi.org/10.1016/B978-0-12-816009-1.00014-9.
Torquato, R.J., 1971. The Damara system in Angola (some preliminary observations on the existence of two geosyncline facies). Rel. Comun. Inst. Invest. Cient. Angola 13, 5–27.
Torquato, J., 1974. Algumas considerações sobre a idade do grupo chela. Dir. Prov. Serv. Geol. Minas Angola 14, 1–10.
Torquato, J., Salgueiro, M., 1977. Sobre a idade de algumas rochas da região da Cahama (folha geológica n° 399): Angola. Bol. Inst. Geocienc. USP 8, 97–106. https://doi.org/10.11606/issn.2316-8978.v8i0p97-106.
Tshiningayamwe, M., Bolhar, R., Nex, P., 2022. Petrology, geochemistry and new U-pb ages of the epembe syenites and carbonatite, northwest Namibia. J. Afr. Earth. Sci. 196,. https://doi.org/10.1016/j.jafrearsci.2022.104719 104719.
Vale, F.S., 1973a. Notícia explicativa da carta geológica de Angola, folha 356 (Vila João de Almeida), escala 1:100.000. Dir. Prov. Serv. Geol. Minas Angola, Luanda.
Vale, F.S., 1973b. Notícia explicativa da carta geológica de Angola, folha 355 (Humpata-Cainde), escala 1:100.000. Dir. Prov. Serv. Geol. Minas Angola, Luanda.
Vermeesch, P., 2012. On the visualisation of detrital age distributions. Chem. Geol. 312–313, 190–194. https://doi.org/10.1016/j.chemgeo.2012.04.021.
Vermeesch, P., 2013. Multi-sample comparison of detrital age distributions. Chem. Geol. 341, 140–146. https://doi.org/10.1016/j.chemgeo.2013.01.010.
Vermeesch, P., 2018. IsoplotR: a free and open toolbox for geochronology. Geosci. Front. 9, 1479–1493. https://doi.org/10.1016/j.gsf.2018.04.001.
Vermeesch, P., 2021a. On the treatment of discordant detrital zircon U-pb data. Geochronology 3, 247–257. https://doi.org/10.5194/gchron-3-247-2021.
Vermeesch, P., 2021b. Maximum depositional age estimation revisited. Geosci. Front. 12, 843–850. https://doi.org/10.1016/j.gsf.2020.08.008.
Vermeesch, P., Garzanti, E., 2015. Making geological sense of 'big data' in sedimentary provenance analysis. Chem. Geol. 409, 20–27. https://doi.org/10.1016/j.chemgeo.2015.05.004.
Vervoort, J., Kemp, A., 2016. Clarifying the zircon hf isotope record of crust–mantle evolution. Chem. Geol. 425, 65–75. https://doi.org/10.1016/j.chemgeo.2016.01.023.
Vorster, C., 2013. Laser Ablation ICP-MS Age Determination of Detrital Zircon Populations in the Phanerozoic Cape and Lower Karoo Supergroups (South Africa) and Correlatives in Argentina (PhD thesis. University of Johannesburg, Johannesburg, South Africa. https://hdl.handle.net/10210/8789.
Williams, I., 1998. U-Th-Pb Geochronology by Ion Microprobe. In: McKibben, M., Shanks, W.C.I., Ridley, W. (Eds.), Reviews in Economic Geology, Applications of Microanalytical Techniques to Understanding Mineralizing Processes. Society of Economic Geologists, 1–35. Doi: Doi: 10.5382/Rev.07.01.
Wissink, G., Wilkinson, B., Hoke, G., 2018. Pairwise sample comparisons and multidimensional scaling of detrital zircon ages with examples from the north American platform, basin, and passive margin settings. Lithosphere 10 (3), 478–491. https://doi.org/10.1130/L700.1.
Woodhead, J., Hergt, J., 2005. A Preliminary appraisal of seven natural zircon reference materials for in situ hf isotope determination. Geostand. Geoanal. Res. 29, 183–195. https://doi.org/10.1111/j.1751-908X.2005.tb00891.x.
Wu, G., Yang, S., Meert, J., Xiao, Y., Chen, Y., Wang, Z., Li, X., 2020. Two phases of paleoproterozoic orogenesis in the Tarim craton: implications for Columbia assembly. Gondwana Res. 83, 201–216. https://doi.org/10.1016/j.gr.2020.02.009.
Xu, Y., Cawood, P., Du, Y., Hu, L., Yu, W., Zhu, Y., Li, W., 2013. Linking south China to northern Australia and India on the margin of Gondwana: constraints from detrital zircon U-pb and hf isotopes in cambrian strata. Tectonics 32, 1547–1558. https://doi.org/10.1002/tect.20099.
Zimmermann, U., Andersen, T., Madland, M., Larsen, I., 2015. The role of U-pb ages of detrital zircons in sedimentology—An alarming case study for the impact of sampling for provenance interpretation. Sediment. Geol. 320, 38–50. https://doi.org/10.1016/j.sedgeo.2015.02.006.